© 2021. Published by The Company of Biologists Ltd | Development (2021) 148, dev199421. doi:10.1242/dev.199421

RESEARCH ARTICLE

Glypican 4 regulates planar cell polarity of endoderm cells by controlling the localization of Cadherin 2

Anurag Kakkerla Balaraju, Bo Hu, Juan J. Rodriguez, Matthew Murry and Fang Lin*

ABSTRACT

Noncanonical Wnt/planar cell polarity (Wnt/PCP) signaling has been implicated in endoderm morphogenesis. However, the underlying cellular and molecular mechanisms of this process are unclear. We found that, during convergence and extension (C&E) in zebrafish, gut endodermal cells are polarized mediolaterally, with GFP-Vangl2 enriched at the anterior edges. Endoderm cell polarity is lost and intercalation is impaired in the absence of *glypican 4* (*gpc4*), a heparan-sulfate proteoglycan that promotes Wnt/PCP signaling, suggesting that this signaling is required for endodermal cell polarity. Live imaging revealed that endoderm C&E is accomplished by polarized cell protrusions and junction remodeling, which are impaired in *gpc4*-deficient endodermal cells. Furthermore, in the absence of *gpc4*, Cadherin 2 expression on the endodermal cell surface is increased as a result of impaired Rab5c-mediated endocytosis, which partially accounts for the endodermal defects in these mutants. These findings indicate that Gpc4 regulates endodermal planar cell polarity during endoderm C&E by influencing the localization of Cadherin 2. Thus, our study uncovers a new mechanism by which Gpc4 regulates planar cell polarity and reveals the role of Wnt/PCP signaling in endoderm morphogenesis.

KEY WORDS: Glypican 4, Planar cell polarity, Endoderm convergence and extension, Cadherin 2, Zebrafish

INTRODUCTION

The endoderm contributes to the development of gastrointestinal tracts (Zorn and Wells, 2009). Although the morphogenetic processes that transform the naive endoderm into a primitive gut tube differ among organisms, in both mice and zebrafish the endoderm and other germ layers undergo convergence and extension (C&E) during gastrulation, which elongate and narrow the body axis (Garcia-Garcia et al., 2008; Spence et al., 2011). These early C&E events pave the way for additional morphogenetic changes that ultimately form the primitive gut-tube (Ober et al., 2003; Zorn and Wells, 2009). Compared with the cellular and molecular mechanisms that control C&E of the mesoderm, those involved in endoderm morphogenesis are not well understood, in part because of limitations of *in vivo* imaging and the complexity of morphogenetic events that arise among germ layers.

In zebrafish, once endodermal cells are derived from the mesoendoderm lineages they become enlarged and exhibit a distinct flat morphology with multiple cellular protrusions that is different from the morphology of mesodermal cells (Warga and Nüsslein-Volhard, 1999). Subsequently, at the onset of gastrulation, endodermal cells engage in a cell-autonomous 'random walk', in which cells migrate without specific directionality (Pezeron et al., 2008). During gastrulation, endodermal cells undergo C&E similar to mesodermal cells, although these movements are regulated by distinct signaling pathways: chemokine signaling regulates the migration of endodermal but not mesodermal cells, whereas Wnt/planar cell polarity (Wnt/PCP) signaling regulates the migration of mesodermal and ectodermal but not endodermal cells (Mizoguchi et al., 2008; Nair and Schilling, 2008), suggesting that the migration of mesodermal and endodermal cells is independent.

During segmentation, endodermal cells in the posterior region of zebrafish embryo (gut endoderm) form a monolayer sheet, which undergoes C&E to converge and elongate, forming the gut tube and its associated organs by 2 days post fertilization (day 2) (Ober et al., 2003; Wallace and Pack, 2003). Impaired endoderm C&E at segmentation is observed in zebrafish with mutations in *Van Gogh-like 2* (*vangl2*, which encodes a Wnt/PCP core protein) and *glypican 4* [*gpc4*, which encodes a heparan-sulfate proteoglycan (HSPG) that influences Wnt/PCP signaling] (Miles et al., 2017). Both *vangl2* and *gpc4* mutants exhibit mesoderm C&E defects at gastrulation, which result from impaired polarity and directed migration of mesodermal cells (Jessen et al., 2002; Topczewski et al., 2001). Thus, Wnt/PCP signaling is involved in both mesoderm and endoderm C&E in zebrafish.

Notably, Wnt/PCP signaling is also implicated in early mouse development, including endoderm C&E (Wen et al., 2010) and is required for gut formation in both mouse and *Xenopus*. Specifically, gut elongation is impaired in Wnt/PCP mutant mice [i.e. those harboring mutant forms of Wnt5a, its receptor Ror2 and the secreted Frizzled-related protein (Sfrp1)] (Cervantes et al., 2009; Matsuyama et al., 2009; Yamada et al., 2010). Likewise, in *Xenopus*, Sfrp, Vangl2, as well as Rho/ROCK and Jun N-terminal kinase (both downstream of Wnt/PCP signaling), are crucial for endodermal cell rearrangement and gut elongation (Dush and Nascone-Yoder, 2013; Reed et al., 2009; Yin et al., 2008). However, polarity of endodermal cells has not been detected in zebrafish (Miles et al., 2017), which brings into question whether endodermal cells migrate actively and how Wnt/PCP signaling regulates endoderm C&E.

In this study, we addressed this question by using high-resolution imaging using our recently generated transgenic zebrafish lines in which the endodermal cell membrane and nucleus are fluorescently labeled (Hu et al., 2020 preprint). We report that, at segmentation, when the endoderm undergoes C&E, endodermal cells progressively polarize along the mediolateral (ML) axis and GFP-tagged Vangl2 is localized asymmetrically at their anterior edges. The endodermal polarity is lost in *gpc4* mutants, indicating that endodermal cells exhibit planar polarity that is dependent on Wnt/PCP signaling. Furthermore, live imaging reveals that

Department of Anatomy and Cell Biology, Carver College of Medicine, The University of Iowa, Iowa City, IA 52242, USA.

*Author for correspondence (fang-lin@uiowa.edu)

F.L., 0000-0003-2179-7031

Handling Editor: Steve Wilson
Received 28 January 2021; Accepted 9 June 2021

Development (2021) 148, dev199421. doi:10.1242/dev.199421

gpc4-deficient cells lose polarized protrusions and display impaired junctional changes, resulting in the formation of excess rosettes, which may interfere with efficient C&E. Mechanistically, our results show that Gpc4 regulates endodermal cell polarity by affecting Rab5c-mediated endocytosis of Cadherin 2 (Cdh2; N-cadherin) to modulate its expression on the cell surface. Collectively, these results elucidate a new mechanism by which Gpc4 regulates polarized cell behaviors during endoderm C&E movement.

RESULTS

Gpc4 is required for planar polarization of endodermal cells during segmentation

During segmentation, the gut endoderm undergoes C&E to narrow and elongate the tissue along the embryonic midline, forming the gut-tube (Ober et al., 2003). Similar to an earlier report (Miles et al., 2017), by using a transgenic line, *Tg(sox17:EGFP)*, in which endoderm is labeled with EGFP, we found that, throughout segmentation, the endodermal sheet is wider in $gpc4^{-/-}$ embryos than in sibling controls (Fig. S1). In addition, we observed an enlarged gut-tube and malformed digestive organs in $gpc4^{-/-}$ embryos at day 2 (Fig. S1). Thus, Gpc4 is required for endoderm C&E and proper gut formation.

To determine the cellular basis of endoderm C&E and how Gpc4 affects this process, we analyzed the morphology of endodermal cells at different stages in embryos obtained from crossing $gpc4^{+/-}$/*Tg(sox17:memGFP/H2A-mCherry)* zebrafish lines (in which the plasma membrane and nuclei of endodermal cells are labeled with GFP and mCherry, respectively) (Hu et al., 2020 preprint) (Fig. 1). We found that, during these stages, endodermal cells in control embryos underwent dramatic changes in cell shape. At the tailbud stage (TB), endoderm cells were not polarized and were loosely packed without apparent cell-cell contact (Fig. 1A); at the 6-12 somite (s, 6-12s) stage, endoderm cells formed cell-cell contacts, became progressively elongated and aligned

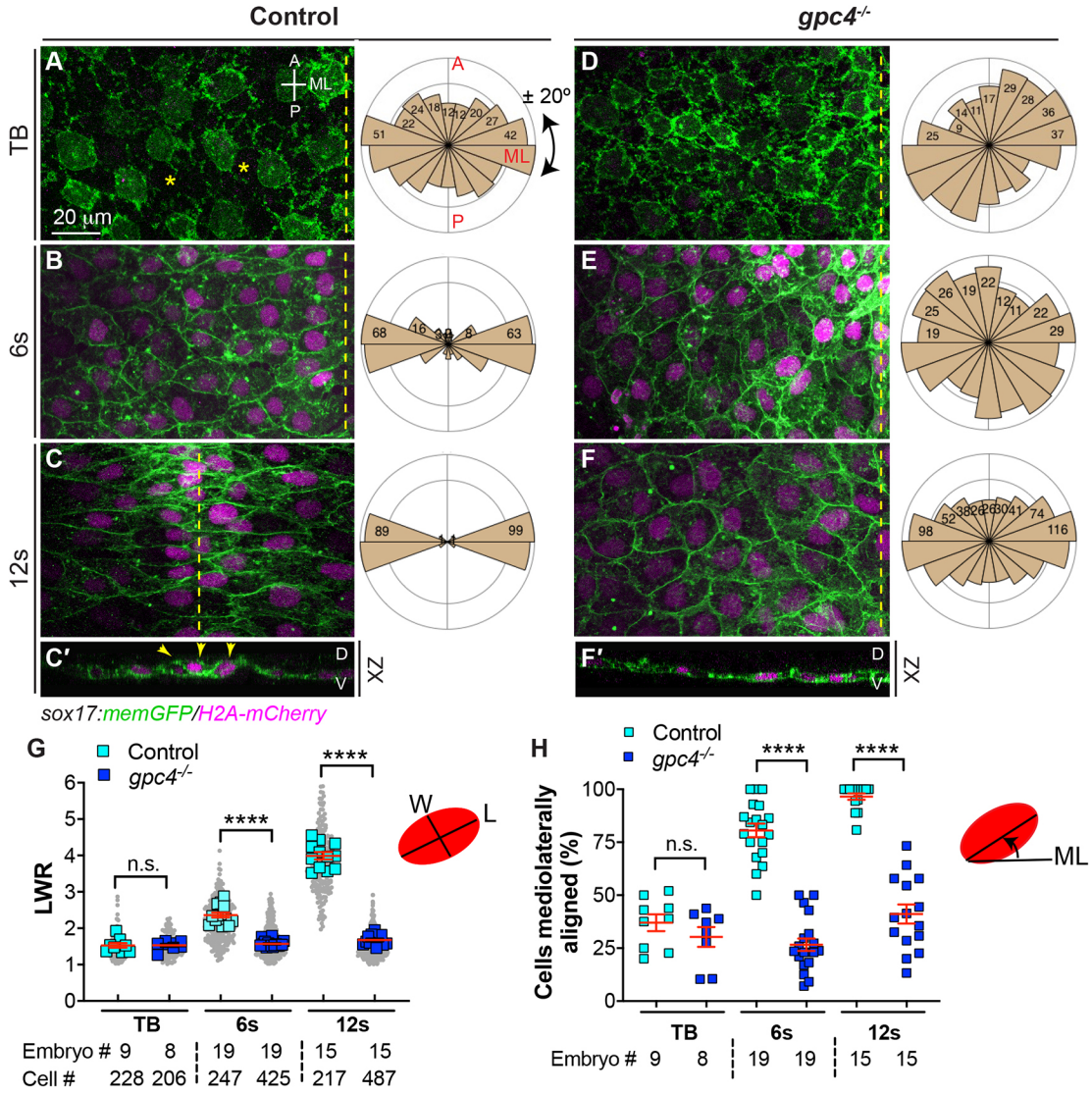

Fig. 1. Gpc4 is required for endodermal cell polarity during segmentation. (A-F′) Confocal images showing endodermal cells with plasma membrane (GFP) and nuclei (pseudo-colored magenta) labeled in the indicated embryos at the tailbud (TB), 6s and 12s stages. (A-F) *Z*-projection of XY view; (C′,F′) *Z*-projection of XZ view. Asterisks indicate gaps between cells; dashed-yellow lines indicate the midline. A, anterior; D, dorsal; ML, mediolateral; P, posterior; V, ventral. Rose plots illustrate the cell orientation in indicated embryos (each bin, 20°). (G) Average length-to-width ratio (LWR) of endodermal cells in embryos in A-F. Data from all embryos (squares) and all cells (gray circles) are superimposed, with the number of cells and embryos indicated. (H) Percentage of cells the longitudinal axis of which was oriented ±20° with respect to the ML embryonic axis in embryos in A-F. Data are mean±s.e.m. n.s., not significant, $P>0.05$, ****$P<0.0001$ (unpaired, two-tailed Student's *t*-test).

Development (2021) 148, dev199421. doi:10.1242/dev.199421

along the ML axis (Fig. 1B,C). To analyze the shape of endodermal cells, we measured the length-to-width ratio (LWR), in which the length and width were the longest measurable distances along each cellular axis (D'Souza-Schorey, 2005). We found that the LWR was 1.49 at TB and increased from 2.31 at the 6s stage to 3.91 at the 12s stage (Fig. 1G). To analyze the orientation of endodermal cells, we measured the angle of their long axes with respect to the ML axis of the embryo and plotted them in rose diagrams (Topczewski et al., 2001). At TB, endodermal cells lacked a particular orientation and 37% of them oriented their long axes within ±20° of the ML axis; at the 6s-12s stages, endodermal cells gradually oriented mediolaterally, with 80-97% of cells aligned within ±20° of the ML axis (Fig. 1A-F,H). Thus, between the TB and 12s stages, endodermal cells progressively elongated and polarized along the ML axis across the entire endodermal sheet, indicating that these cells exhibit PCP during endoderm C&E.

In *gpc4*$^{-/-}$ embryos, at TB, endodermal cells also did not exhibit obvious polarity and showed similar LWR and ML alignment to their control counterparts (Fig. 1D,G,H). However, these cells were tightly packed with clear cell adherent boundaries and lacked the gaps between cells seen in control endoderm (Fig. 1D versus Fig. 1A), suggesting that cell-cell adhesion in these cells is increased. From the 6s to the 12s stage, *gpc4*-deficient endodermal cells were round and lacked obvious polarity; their LWRs were significantly lower (P<0.0001; unpaired, two-tailed Student's t-test) and fewer cells were aligned along the ML axis (Fig. 1D-H). In addition, we further examined cell polarity by assessing expression of γ-tubulin in endodermal cells, which labels microtubule organizing centers (MTOCs), an indicator of cell polarity (Sepich et al., 2011). At 10s, MTOCs were located at the front or lateral sides of nuclei in control endodermal cells that were elongated, but were randomly positioned in *gpc4*$^{-/-}$ cells (Fig. S2A,B). To quantify the relative position of MTOCs with the nucleus of endodermal cells, we assessed the angle of the line drawn from the MTOC to the center of the nucleus relative to the ML axis (Fig. S2C). Rose plots revealed that 60.9% of MTOCs in control cells were aligned within ±20° of the ML axis, whereas this pattern was observed in only 20.3% of MTOCs in *gpc4*$^{-/-}$ endodermal cells (Fig. S2D,E). Taken together, these data indicate that endodermal cells exhibit planar polarity during endoderm C&E at early and mid-segmentation and that this requires Gpc4.

Notably, although the endoderm completed C&E at the ∼18s stage (Fig. S1), confocal imaging revealed that endodermal cells underwent C&E as a monolayer until the 12s stage (Fig. 1C′,F′), which is consistent with an earlier report (Miles et al., 2017). After that, endodermal cells appeared to change their behavior: they moved ventrally (the apical side) and became constricted apically, forming a rod structure with a central point at 16-21 s (Fig. S3A,C). By day 2, the endoderm formed a gut-tube with a central lumen enriched with actin (Fig. S3G-H′), which was consistent with previously published reports (Horne-Badovinac et al., 2001; Wallace and Pack, 2003). Thus, endoderm cells exhibit different cell behaviors from the TB to 12s stage and after the 12s stage. In *gpc4*$^{-/-}$ embryos, although the endoderm sheet was wider, cells also moved ventrally, but formed multiple center points (Fig. S3B,D) and developed a gut-tube with multiple disconnected and misformed lumen (Fig. S3I-J′). Thus, Gpc4 is required for polarity and intercalation, but not apical constriction, of endodermal cells during endoderm C&E.

Gpc4 is required for planar polarity of endodermal cells in both cell-autonomous and non-cell-autonomous manners

Gpc4 regulates the planar polarity of gastrulating mesodermal cells during C&E (Topczewski et al., 2001); thus, Gpc4 is required for C&E of both mesoderm and endoderm. Our previous study showed that the *gpc4* transcript is present in the endoderm and that endodermal expression of GFP-Gpc4 completely rescues endodermal defects in *gpc4*-deficient embryos (Hu et al., 2020 preprint), indicating that its expression in endoderm is sufficient to suppress endoderm defects observed in *gpc4*$^{-/-}$ embryos. These data suggest that Gpc4 functions in the endoderm. To test whether Gpc4 regulates endodermal cell polarity in a cell-autonomous manner, we performed endoderm transplantation experiments to generate chimeric endoderm in which control and *gpc4*-deficient cells contact each other. Embryos derived from incrossing *gpc4*$^{+/-}$/*Tg(sox17:memGFP/H2A-mCherry)* fish were used as both donors and hosts (all embryos were genotyped). Donor embryos were injected with *h2b-GFP* RNA to mark the nuclei of donor cells with GFP (Fig. 2A). Confocal imaging was performed on the host endoderm transplanted with donor endoderm cells, and LWR and ML alignments of donor and host cells were analyzed.

Transplanted control donor endodermal cells displayed morphology and LWR comparable with control host endoderm cells (Fig. 2B), whereas transplanted *gpc4*$^{-/-}$ donor endodermal cells displayed cell morphology similar to that of *gpc4*$^{-/-}$ host endoderm cells (Fig. 2C). These data demonstrate that our transplantation procedure did not impair the morphology of either the donor or host endodermal cells. However, control donor endoderm cells lost their polarity when transplanted into *gpc4*$^{-/-}$ hosts and instead exhibited a round cell shape similar to that of host cells (Fig. 2D), suggesting that control endoderm cells were affected by the surrounding *gpc4*$^{-/-}$ cells. In addition, we conducted reverse transplantation, in which *gpc4*$^{-/-}$ endodermal cells were transplanted into control hosts. Donor *gpc4*$^{-/-}$ endodermal cells displayed a range of cell morphologies, with their LWR distributed in a bimodal pattern: some cells were clustered together and remained round with an LWR similar to that of mutant cells (pattern 1, Fig. 2E,H), whereas some donor cells that were scattered among host cells were more elongate, with an LWR similar to that of normal control host cells (pattern 2, Fig. 2F,H). Notably, we also observed differences in the cell shape of host endodermal cells, depending on whether they had direct contact with donor *gpc4*$^{-/-}$ cells. Control host cells adjacent to donor *gpc4*$^{-/-}$ cells (white dots in Fig. 2E) had a more-rounded shape and their LWR did not differ significantly from that of the round donor *gpc4*$^{-/-}$ cells (asterisks in Fig. 2E; see also Fig. 2H; P>0.05; unpaired, two-tailed Student's t-tests). In contrast, control cells that were far away from donor *gpc4*$^{-/-}$ cells remained elongated (white dots in Fig. 2G versus Fig. 2B), similar to those cells that were transplanted among control cells (Fig. 2G versus Fig. 2B; see also Fig. 2H). These findings indicate that, although *gpc4*$^{-/-}$ cells can maintain their cell morphology, their shape is influenced by, and they can also impair the polarity of, neighboring cells. Thus, both *gpc4*-deficient cells and control cells influence each other, suggesting that Gpc4 regulates planar polarity of endodermal cells in a cell-autonomous and non-cell-autonomous manner.

Gpc4 is required for efficient mediolateral endodermal cell intercalation

C&E of many cell types can be driven by cell intercalation, in which neighboring cells exchange places in either the same or different planes (Walck-Shannon and Hardin, 2014). Cell intercalation is achieved by cell-on-cell traction, which is mediated by polarized protrusive activity and/or shrinking cell junctions (Huebner and Wallingford, 2018; Keller et al., 2000; Keller and Sutherland, 2020; Shindo and Wallingford, 2014). To understand the cellular mechanisms underlying endoderm C&E and how Gpc4 regulates

Development (2021) 148, dev199421. doi:10.1242/dev.199421

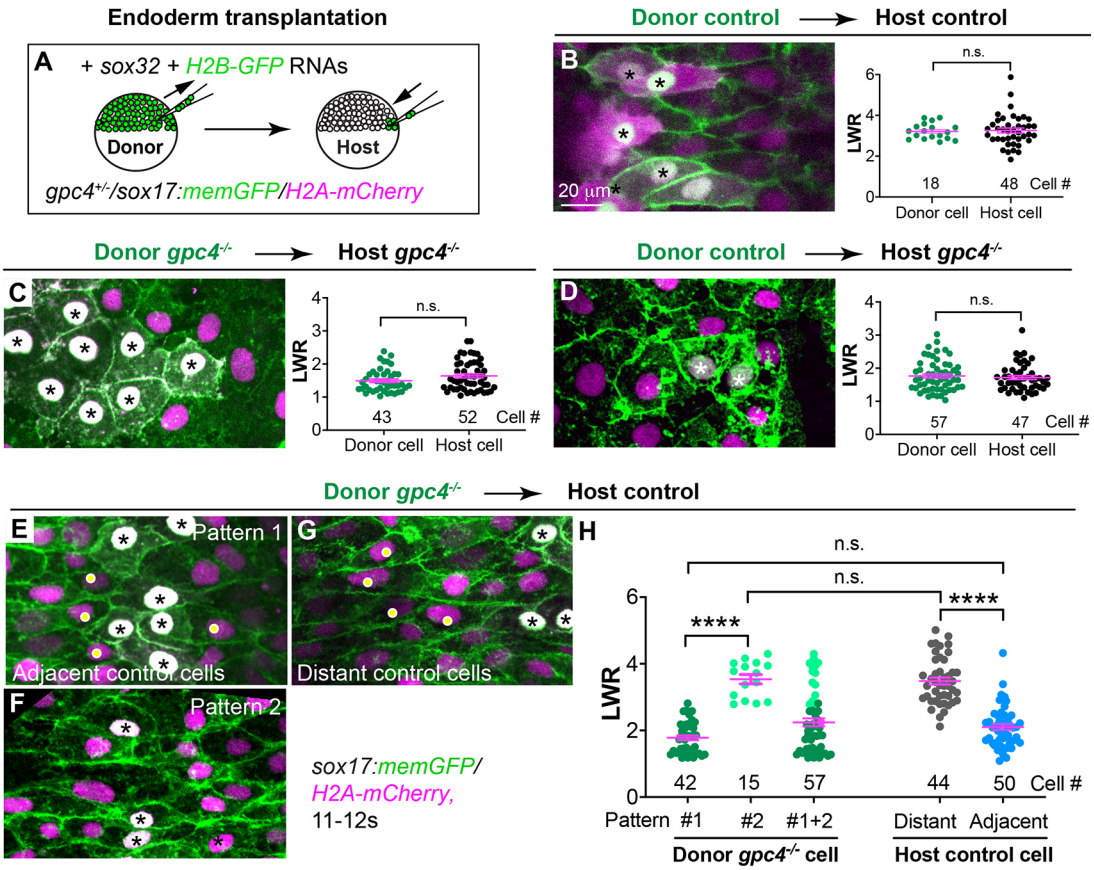

Fig. 2. Gpc4 is required in a cell-autonomous and non-cell-autonomous manner for planar polarity of endodermal cells. (A) Schematic illustrating endoderm transplantation in embryos obtained from incrossing *gpc4*$^{+/-}$/*sox17:memGFP*/*H2A-mCherry* zebrafish. (B-G) XY view confocal images (*Z*-projection) showing endoderm in the indicated host embryos transplanted with the indicated donor endoderm cells (the nuclei of which are white, indicated by asterisks). Graphs show average LWR of host (green) and donor (black) endodermal cells at the 12s stage of control donor cells transplanted into sibling control hosts (B, four embryos); *gpc4*$^{-/-}$ donor cells transplanted into *gpc4*$^{-/-}$ hosts (C, five embryos); and control donor cells transplanted into *gpc4*$^{-/-}$ hosts (D, three embryos). (E-G) XY view confocal images (*Z*-projection) showing endodermal cells displaying different patterns in control hosts transplanted with *gpc4*$^{-/-}$ cells (nine embryos). Yellow dots show control host cells. (H) Average LWR of host and donor endodermal cells at the 12s stage. All cells analyzed are plotted and the number of cells is shown. Dark green dots, pattern 1 donor cells; light green dots, pattern 2 donor cells; grey dots, distant host cells; blue dots, host cells adjacent to donor cells. Data are mean±s.e.m. n.s., not significant, $P>0.05$; ****$P<0.0001$ (unpaired, two-tailed Student's *t*-test).

them, we performed confocal time-lapse imaging at the 6s-12s stages, at which the endoderm is visible under a confocal microscope. Tracking cell movements revealed (Keller and Sutherland, 2020) that, in control embryos, endodermal cells migrated from the lateral region toward the midline while also intercalating mediolaterally, thereby exchanging their relative positions and narrowing and extending the endodermal sheet (Fig. S4, Movie 1). In addition, we found that endodermal cells exhibited two types of behavior during intercalation. Some cells remodeled their cell junctions: the ML junction (Type 3, T3; Fig. 3C1) shortened mediolaterally to allow two cells (#1, #4) to meet to form a center point (Type 2, T2) with two neighboring cells (#2, #3, Fig. 3C2); then, a new junction formed along the anterior-posterior (AP) axis (Type 1, T1), which separated these cells (#2, #3, Fig. 3C3). Occasionally, the ML junctions of five to six endodermal cells shortened to form a common vertex, developing a multicellular rosette (Fig. 3A,A′), whereas some cells extended cellular protrusions, squeezed between two neighboring cells, and changed their position among the adjacent cells (red arrows, Fig. 3C2-C4, Movie 1). To better visualize these protrusions, we conducted time-lapse imaging at higher magnification and found that these protrusions were present mainly along the ML axis at both leading and trailing edges (Movie 2, Fig. 3J), with 43±7% of these protrusions being aligned within ±20° of the ML axis (Fig. 3J′). In addition, time-lapse imaging was conducted in mosaically labeled transplanted endodermal cells. In this setting, ML protrusions were evident (Fig. S5). Notably, we found some protrusions extended into the shortening-ML junctions of the neighboring cells (Fig. S5A-C, Movie 3). Analyzing the relative positions of cell protrusions and shortening-ML junctions revealed that they were not located in the same *z*-planes, with the contracting ML junctions appearing to be located dorsally relative to the cellular protrusions (Fig. S5D,E). In addition, we observed that protrusion extension and ML junction shortening were not synchronized: when the protrusions retracted back to the cell, the junctional shortening continued. Therefore, our results reveal that both cellular protrusions and shortening-ML junctions co-exist in converging endodermal cells (Fig. S5F). Thus, it is likely that both junctional remodeling and polarized cell protrusions act in concert to drive endodermal cells to intercalate during C&E.

Strikingly, endodermal cells in *gpc4*$^{-/-}$ embryos displayed a honeycomb appearance, with the presence of multiple rosettes and the absence of polarized protrusions (Fig. 3B,B′, Movie 4). However, *gpc4*-deficient endodermal cells underwent similar cell junction remodeling (T3 to T1; Fig. 3D1-D4). Tracking junction changes revealed that, in these cells, some T3 junctions were present for an extended period of time, had a decreased rate of shortening compared with control cells (Fig. 3E) and often did not proceed to the next steps

Development (2021) 148, dev199421. doi:10.1242/dev.199421

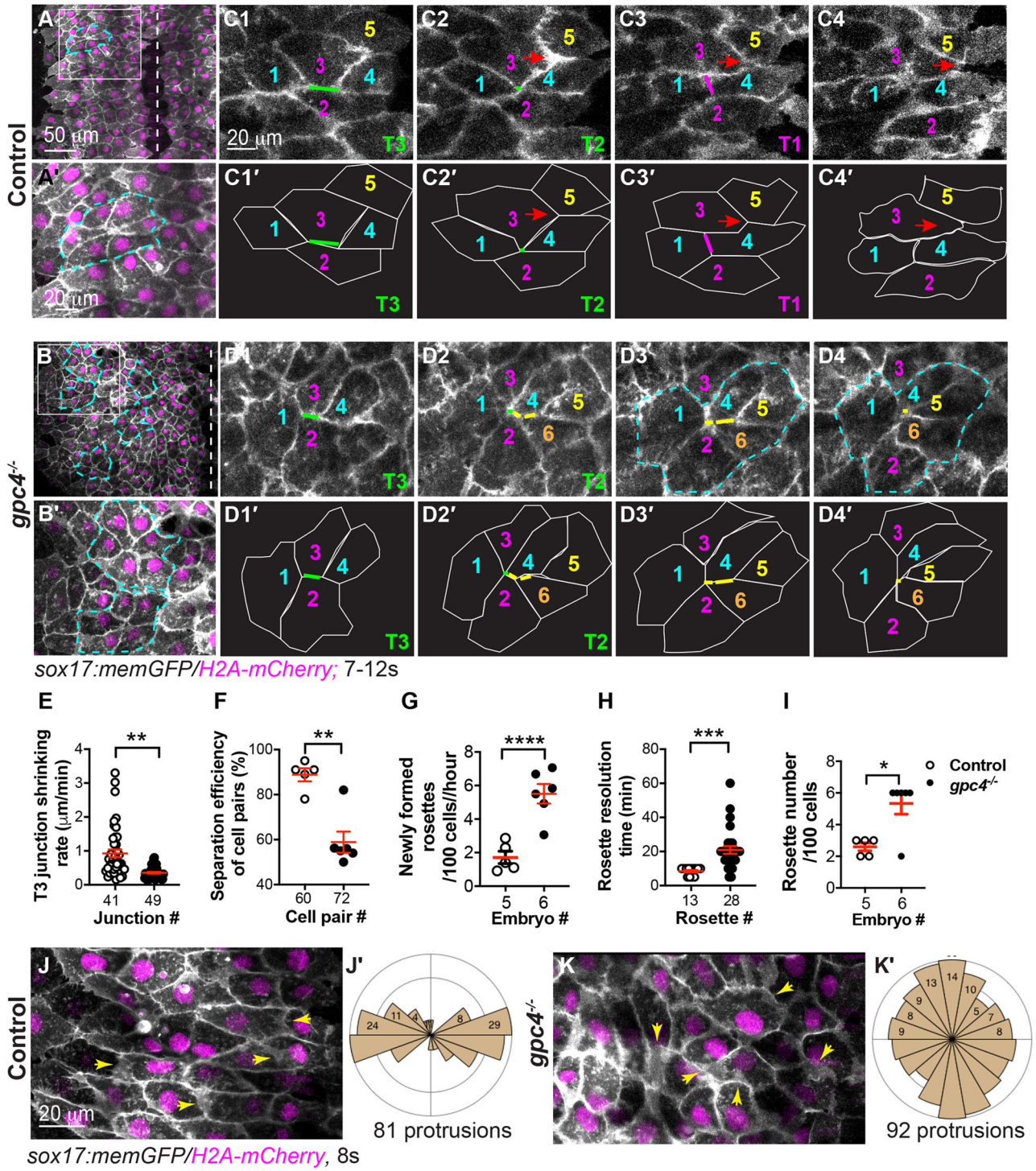

Fig. 3. Gpc4 is required for efficient ML intercalation of endodermal cells. (A-D4′) Confocal time-lapse experiments in control (five embryos) and *gpc4*$^{-/-}$ (six embryos) at the 7s-12s stages using a 20× objective (see Movies 1, 3 and the main text). (A,B) Snapshots from Movies 1 and 3 in the main text showing an overview of one side of the endoderm. Dashed-white lines indicate the midline. (A′,B′) Magnification of region in boxed area in A,B. Dashed-yellow lines indicate rosettes. (C1-D4′) Snapshots from Movies 1 and 3 showing relative positions of some endodermal cells, labeled with the same-colored number over time. Red arrows indicate cells that have squeezed between two neighboring cells; green lines indicate ML junctions (Type 3, T3; C1,C1′,D1,D2,D1′,D2′) shrunk to form a common vertex (Type 2, T2; C2,C2′); magenta line indicates new vertical junctions (Type 1, T1; C3,C3′); yellow lines (D2-D4,D2′-D4′) indicate multiple ML junctions contracting to form rosettes (outlined by dashed-cyan lines; D3,D4). (C1′-C4′,D1′-D4′) Outlines of some of the endodermal cells in C1-C4 and D1-D4 (white lines). (E-H) Quantification of cell behaviors, as represented in C1-C4 and D1-D4. (E) Shrinking rate of the T3 junction (from T3 to T2), with number of junctions analyzed shown. (F) Percentage of cell pairs separated along the AP axis, with number analyzed indicated. (G) Newly formed rosettes per 100 endodermal cells per hour. (H) Resolution time of rosettes formed during the first 60 min of the time-lapse movies (Movies 1, 3), with number analyzed indicated. (H) Total number of rosettes formed per 100 endodermal cells from the 7s-12 s stage. Data are mean±s.e.m. *P<0.05; **P<0.01; ***P<0.001; ****P<0.0001 (unpaired two-tailed Student's t-test). (J-K′) Confocal time-lapse experiments in control (six embryos) and *gpc4*$^{-/-}$ (six embryos) using a 40× oil objective (see Movies 2 and 4). (J,K) Snapshots from Movies 2 and 4. Yellow arrows indicate cell protrusions. (J′,K′) Rose plots showing orientation of cell protrusions in endodermal cells (bin size, 20°).

Development (2021) 148, dev199421. doi:10.1242/dev.199421

(to T2 or T1) during the span of the time-lapse. Instead, some multiple T3 junctions shortened to bring more than four cells to form a rosette (yellow lines, Fig. 3D2-D4). Thus, relative to control cells, fewer T3 junctions in *gpc4*-deficient endodermal cells led to a decrease in the separation of neighboring cells along the AP axis (Fig. 3F). However, *gpc4*-deficient endodermal cells produced significantly more new rosettes (P<0.0001; unpaired, two-tailed Student's *t*-test) (Fig. 3G), which lasted significantly longer (P<0.001; unpaired, two-tailed Student's *t*-test) (Fig. 3H), leading to an increase in total rosette number (Fig. 3I). Notably, at 24s, control endodermal cells had already formed a single rod (Fig. S3E), whereas *gpc4*-deficient endodermal cells still exhibited the rosettes (Fig. S3F), likely leading to the formation of multiple apical focal points in the malformed gut-tube (Fig. S3I,I′). Furthermore, time-lapse movies obtained from high-magnification images showed that cell protrusions were extended in random directions and there were fewer protrusions (16±3% versus 43±7% in control, P<0.01) that were aligned with the ML axis (Fig. 3K,K′, Movie 5). In addition to a lack of cell protrusions, these inefficient junctional changes and excess rosette formation likely impair proper endoderm cell intercalations and C&E in *gpc4*$^{-/-}$ embryos (Fig. S3). Taken together, our findings indicate that Gpc4 is required for maintaining polarized cell protrusions and promoting efficient cell-junction remodeling.

Gpc4 is required for asymmetrical enrichment of Vangl2 in elongated endodermal cells during endoderm C&E

Our data indicate that, during endoderm C&E at the 6s-12s stages, endodermal cells elongate and polarize mediolaterally and undergo ML intercalation, which preferentially separates anterior and posterior neighboring cells (Figs 1, 3). Such preferential contacts between anterior and posterior neighboring cells can be mediated by the asymmetrical location of PCP proteins (Butler and Wallingford, 2017; Ciruna et al., 2006; Yin et al., 2008). Among them, Vangl2 is enriched at the anterior cell membrane (Roszko et al., 2015). To assess the localization of PCP proteins in endodermal cells and determine the effects of *gpc4* deficiency on this pattern of localization, we performed endoderm transplantation assays to label a subset of endodermal cells with GFP-Vangl2 using a transgenic line, *Tg(vangl2:GFP-vangl2)*, which expresses a zebrafish GFP-Vangl2 N-terminal fusion protein from the *vangl2* promoter (Sittaramane et al., 2013). Donor embryos were derived from incrossing *gpc4*$^{+/-}$*/Tg(vangl2:GFP-vangl2/sox17:memCherry)* fish and injected with RNAs encoding *sox32* and *H2B-RFP* (Fig. 2) so that donor endodermal cells were labeled with GFP-Vangl2 and their nuclei were labeled with RFP. Embryos derived from incrossing *gpc4*$^{+/-}$*/Tg(sox17:memCherry)* fish, in which the plasma membrane of endoderm cells was labeled with mCherry, served as hosts (Fig. 4A). Host embryos were screened at the 11s stage for the presence of RFP-labeled nuclei in the gut endoderm region. Confocal images were acquired and analyzed for the localization of GFP-Vangl2. In control donor endodermal cells in control host embryos, GFP-Vangl2 was largely localized on anterior ML boundaries (Fig. 4B,B′). In contrast, *gpc4*$^{-/-}$ donor endodermal cells in *gpc4*$^{-/-}$ host embryos were more rounded, and displayed GFP-Vangl2 expression in the entire cell periphery (Fig. 4C,C′). Notably, *gpc4*$^{-/-}$ donor endodermal cells tended to cluster together, which made it difficult to assess GFP-Vangl2 distribution in individual cells. Nevertheless, we analyzed individual GFP-Vangl2-expressing cells and found that 88.4% of control endodermal cells displayed GFP-Vangl2 on the anterior edge of ML boundaries, compared with only 10.6% of *gpc4*$^{-/-}$ endodermal cells (Fig. 4D).

As an alternative approach to visualize GFP-Vangl2 distribution in endodermal cells, we generated a transgenic line, *Tg(sox17:GFP-vangl2)*, which expressed GFP-Vangl2 in the endoderm under control of the *sox17* promoter (Fig. S6A). We selected a line that displayed normal embryogenesis for the current study. Embryos derived from crossing this line with the *Tg(sox17:memCherry)* line showed that the GFP-Vangl2 signal was detected in mCherry-labeled endoderm, but not in other tissues (Fig. S6B-B″). In addition, analyses of embryos obtained from crossing this line with the *Tg(sox17:EGFP)* line revealed that embryos with endodermal expression of GFP-Vangl2 displayed a similar body axis and endodermal width comparable with their control embryos without the transgene (Fig. S6D-F). These data suggest that, in the *Tg(sox17:GFP-vangl2)* line, expression of GFP-Vangl2 in the endoderm does not affect normal development of either the mesoderm or endoderm.

Confocal imaging showed that, in *Tg(sox17:GFP-vangl2/sox17:memCherry)* embryos, GFP-Vangl2 colocalized with mCherry, demonstrating that it occurs in the plasma membrane of endoderm cells (Fig. S6C-C″). Notably, GFP-Vangl2 expression was primarily enriched at ML boundaries but not on AP boundaries (Fig. 4E,E′), which was consistent with our transplantation results (Fig. 4B-D). In contrast, GFP-Vangl2 was evenly expressed around the entire cell periphery of endodermal cells in *gpc4*$^{-/-}$*/Tg(sox17:GFP-vangl2)* embryos, similar to our transplantation studies (Fig. 4F,F′). Quantification of the maximum intensity of GFP-Vangl2 confirmed that GFP signaling was significantly higher at ML boundaries than at AP boundaries in control, but not in *gpc4*$^{-/-}$, endodermal cells (Fig. 4G; P<0.0001; unpaired, two-tailed Student's *t*-test). Taken together, our results suggest that, during endoderm C&E, *gpc4* deficiency likely disrupts the polarized Wnt-PCP signaling necessary for planar polarity of endodermal cells.

Increased Cdh2 expression in *gpc4*$^{-/-}$ embryos contributes to polarity defects

We next sought to determine the mechanisms underlying defects in endodermal polarity in *gpc4*$^{-/-}$ embryos. We noticed that, at TB, *gpc4*-deficient endodermal cells were tightly packed with little intercellular space and had more prominent cell boundaries compared with sibling cells (Fig. 1A,D), suggesting that cell-cell adhesion is increased. It has been shown that the expression of Cdh2 on the plasma membrane of gastrulating mesoderm cells in *gpc4*$^{-/-}$ embryos is increased (Dohn et al., 2013). Thus, we assessed the expression of Cdh2 in endodermal cells at 6 s by immunostaining when endodermal cells had just formed cell-cell contacts. We found that Cdh2 expression on the plasma membrane of endodermal cells was notably higher in *gpc4*$^{-/-}$ embryos (Fig. 5A-B′). Quantification revealed that the fluorescence intensity of Cdh2 in the endodermal cell membrane of *gpc4*$^{-/-}$ embryos was increased by 65% compared with that in controls (Fig. 5C). However, total Cdh2 protein expression detected by western blotting and the level of *cdh2* transcript detected by qRT-PCR did not differ between control and *gpc4*$^{-/-}$ embryos (Fig. 5D, data not shown). These data suggest that Gpc4 affects the distribution, but not the expression, of Cdh2.

Cdh2 is a classical cell-cadherin molecule with a crucial role in cell polarity and tissue integrity during development and disease (D'Souza-Schorey, 2005; Nishimura and Takeichi, 2009; Radice, 2013). The loss or misexpression of Cdh2 can affect the polarity and migration of various cell types, including those that form the neural tube (Camand et al., 2012; Detrick et al., 1990; Hong and Brewster, 2006; Radice, 2013). Thus, we postulated that increased Cdh2 expression in *gpc4*-deficient endoderm cells might contribute to their impaired polarity. To address this, we determined whether

Development (2021) 148, dev199421. doi:10.1242/dev.199421

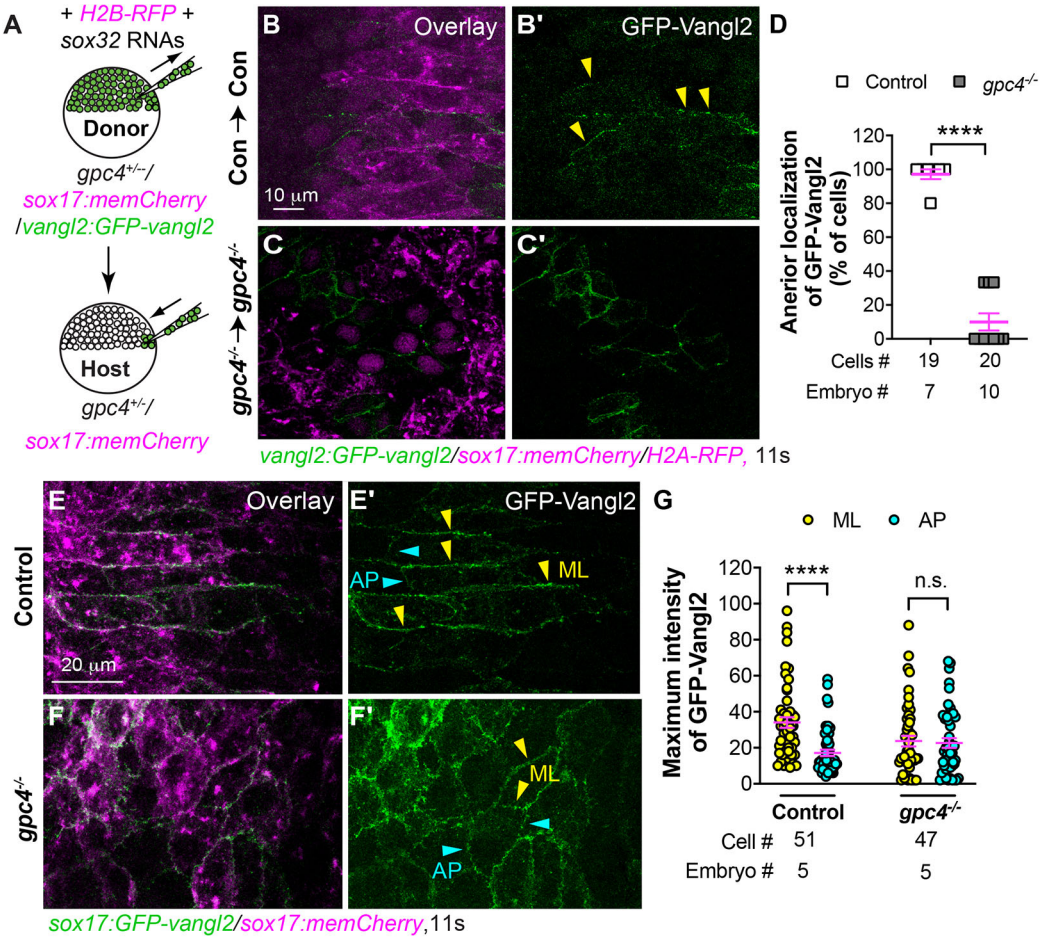

Fig. 4. Vangl2 asymmetrical enrichment in endodermal cells is impaired in *gpc4*$^{-/-}$ embryos. (A) Schematic showing endoderm transplantation. (B-C′) Confocal images showing GFP-Vangl2 distribution in transplanted control endodermal cells in control embryos (B,B′) and transplanted *gpc4*$^{-/-}$ endodermal cells in *gpc4*$^{-/-}$ embryos (C,C′). Yellow arrowheads indicate ML boundaries of endodermal cells. (D) Percentage of donor-endodermal cells expressing GFP-Vangl2 at the anterior ML cell boundary in the indicated host embryos. The number of embryos and cells analyzed is indicated. (E-F′) Confocal images showing GFP-Vangl2 localization in endodermal cells in the indicated embryos. Yellow and cyan arrowheads indicate ML and AP boundaries of endodermal cells, respectively. (G) Maximum intensity of GFP-Vangl2 on ML (yellow) and AP (cyan) boundaries of endodermal cells in the indicated embryos. The number of embryos and cells analyzed is indicated. Data are mean±s.e.m. n.s., not significant, $P>0.05$; ****$P<0.0001$ (unpaired, two-tailed Student's *t*-test).

overexpression of Cdh2 affected endodermal cell polarity. We used endoderm transplantation to overexpress Cdh2-GFP in a subset of endodermal cells by transplanting cells from embryos injected with *cdh2-GFP* mRNA into wild-type (WT) *Tg(sox17:memCherry)* embryos. Cdh2-GFP-expressing donor endodermal cells were more rounded with significantly lower LWR compared with their neighboring WT host endodermal cells (Fig. S7; $P<0.0001$; unpaired, two-tailed Student's *t*-test). Thus, overexpression of Cdh2 in endodermal cells disrupts their cell polarity.

We next asked whether the increased Cdh2 expression in *gpc4*-deficient endodermal cells contributed to their defects in polarity and, thus, tested to see whether reducing Cdh2 expression in *gpc4*$^{-/-}$ embryos suppressed these defects. We injected embryos obtained from *gpc4*$^{+/-}$*/Tg(sox17:memGFP/H2A-mCherry)* fish with a previously published *cdh2* morpholino (MO) to knock down *cdh2* expression (Lele et al., 2002). Injection of a low dose of *cdh2* MO did not cause significant defects in endodermal cell shape in control embryos (Fig. 5E), but did suppress polarity defects in endodermal cells in *gpc4*$^{-/-}$ embryos (Fig. 5F). Quantification revealed that *cdh2*-MO injection improved LWR and cell orientation in endodermal cells of *gpc4*$^{-/-}$ embryos injected with *cdh2*-MO relative to those that were not injected (i.e. LWR 2.2 versus 1.64, respectively, and cells with ML orientation ranging from 77.4% to 48%; Fig. 5I,J). In *cdh2*$^{-/-}$ embryos, endoderm morphogenesis appeared to be normal because endodermal width was comparable with that of their siblings throughout segmentation; endodermal cell shape was also normal (Fig. 5G,I,J; not shown). This suggests that Cdh2 is dispensable for endoderm morphogenesis. To test the impact of genetic deficiency of *cdh2* on endodermal polarity in *gpc4*$^{-/-}$ embryos, we generated double *gpc4/cdh2* mutants. Similar to embryos injected with a *cdh2*-MO, loss of one or both *cdh2* alleles in *gpc4*$^{-/-}$ embryos resulted in endodermal cells that were more elongated and better aligned mediolaterally (Fig. 5H versus Fig. 5G,I,J). To test whether Cdh2 regulates endodermal cell polarity in a cell-autonomous fashion, we transplanted donor cells from *gpc4*$^{-/-}$ embryos injected with *cdh2*-MO into control and *gpc4*$^{-/-}$ embryos. Analyses of cell morphology showed that, in control hosts, although LWR in *gpc4*$^{-/-}$*/cdh2*-MO endodermal cells was lower than that in host control endodermal cells, it was significantly higher than that in *gpc4*$^{-/-}$ endodermal cells ($P<0.0001$; one-way ANOVA, Tukey's multiple comparison test); similarly, in *gpc4*$^{-/-}$ host embryos, *gpc4*$^{-/-}$*/cdh2*-MO endodermal cells displayed significantly higher LWR compared with their neighboring *gpc4*$^{-/-}$ endodermal cells (Fig. S8A-C; $P<0.0001$; unpaired, two-tailed Student's *t*-test). These data indicate that

Development (2021) 148, dev199421. doi:10.1242/dev.199421

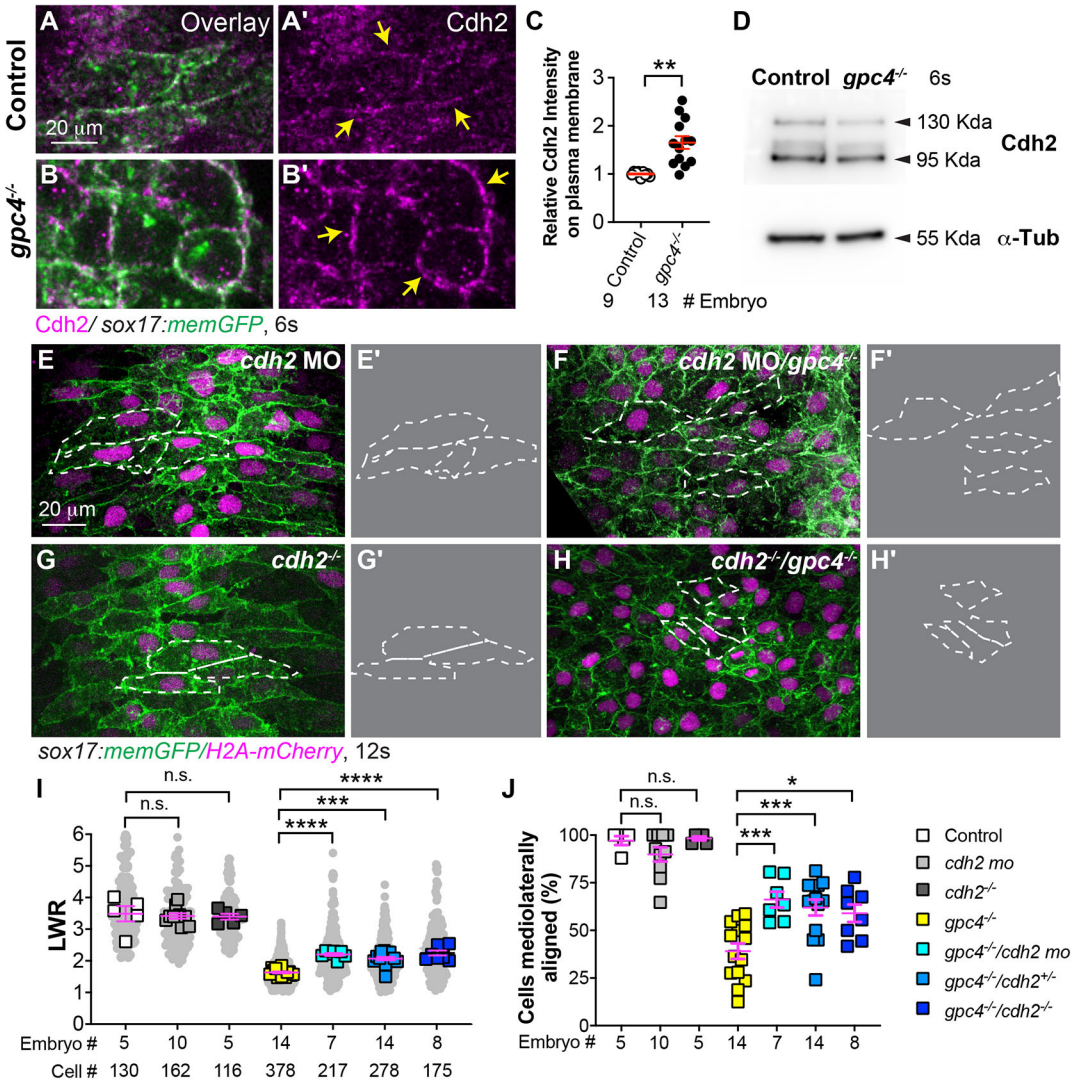

Fig. 5. Suppressing Cdh2 expression partially rescues polarity defects in *gpc4*-deficient endodermal cells. (A-B′) Confocal images (*Z*-projections) showing expression of Cdh2 (magenta, detected by immunostaining) of endodermal cells of the indicated embryos. (C) Relative intensity of Cdh2 expression on the plasma membrane of endodermal cells (yellow arrows) in embryos in A-B′. The number of embryos analyzed is indicated. ***P*<0.01 (unpaired, two-tailed Student's *t*-test). (D) Western blot showing expression of Cdh2 and α-Tubulin (internal control) at the 6s stage (representative of three biological replicates). (E-H′) Confocal images (*Z*-projections) showing endodermal cells in the embryos indicated. (E′,F′,G′,H′) Outlines of some endodermal cells in E,F,G,H (dashed-white lines). (I) Average length-to-width ratio (LWR) of endodermal cells in E-H. Data from all embryos (squares) and all cells (gray circles) are superimposed, with the number of cells and embryos indicated. (J) Percentage of ML-aligned endodermal cells in E-H. Data are mean±s.e.m. One-way ANOVA followed by a Tukey's multiple comparisons test: n.s., not significant, *P*>0.05, **P*<0.05, ****P*<0.001, *****P*<0.0001.

reducing Cdh2 expression in endodermal cells suppressed polarity defects of *gpc4*-deficient endodermal cells, further demonstrating that increased Cdh2 expression is partially responsible for defective endodermal cell polarity in *gpc4*$^{-/-}$ embryos.

Gpc4 regulates Rab5c-mediated endocytosis to control Cdh2 expression on the cell surface

Next, we sought to determine the mechanism by which Gpc4 regulates Cdh2 distribution. The distribution/expression of Cdh2 can be regulated by trafficking (Lindsay and McCaffrey, 2017; Nagaoka et al., 2014; Piloto and Schilling, 2010). To better visualize the distribution of Cdh2 in endodermal cells, we performed confocal imaging at higher magnification (63× oil objective). In addition to the plasma membrane, we detected Cdh2 expression in punctate cytoplasmic structures of endodermal cells (Fig. 6A,A′). In addition, we found the cytoplasmic Cdh2 puncta were colocalized with Eea-1 (Fig. 6D-D″), a marker of early endocytosis (Mu et al., 1995), suggesting that Cdh2 is actively internalized in endodermal cells. Compared with controls, the number of both Cdh2-expressing and Eea-1-positive puncta in the cytosol of *gpc4*-deficient endodermal cells was significantly reduced (Fig. 6A-C′,F-G′; *P*<0.0001; unpaired, two-tailed Student's *t*-test) and colocalization of Cdh2 with Eea-1 was not obvious (Fig. 6E-E″). These data suggest that early endocytosis is impaired in the absence of Gpc4.

Endosomal trafficking is regulated by distinct Rab GTPases and Rab5 is shown to regulate the formation of early endosomes, promoting endocytosis (Zerial and McBride, 2001). We next sought to test whether inhibiting early endocytosis could disrupt endoderm morphogenesis during segmentation. Therefore, we injected WT embryos with mRNA to express RN-tre, a GTPase-activating protein that specifically inhibits Rab5 activity by converting it into Rab5-GDP (Scholpp and Brand, 2004). Our results showed that overexpression of

Development (2021) 148, dev199421. doi:10.1242/dev.199421

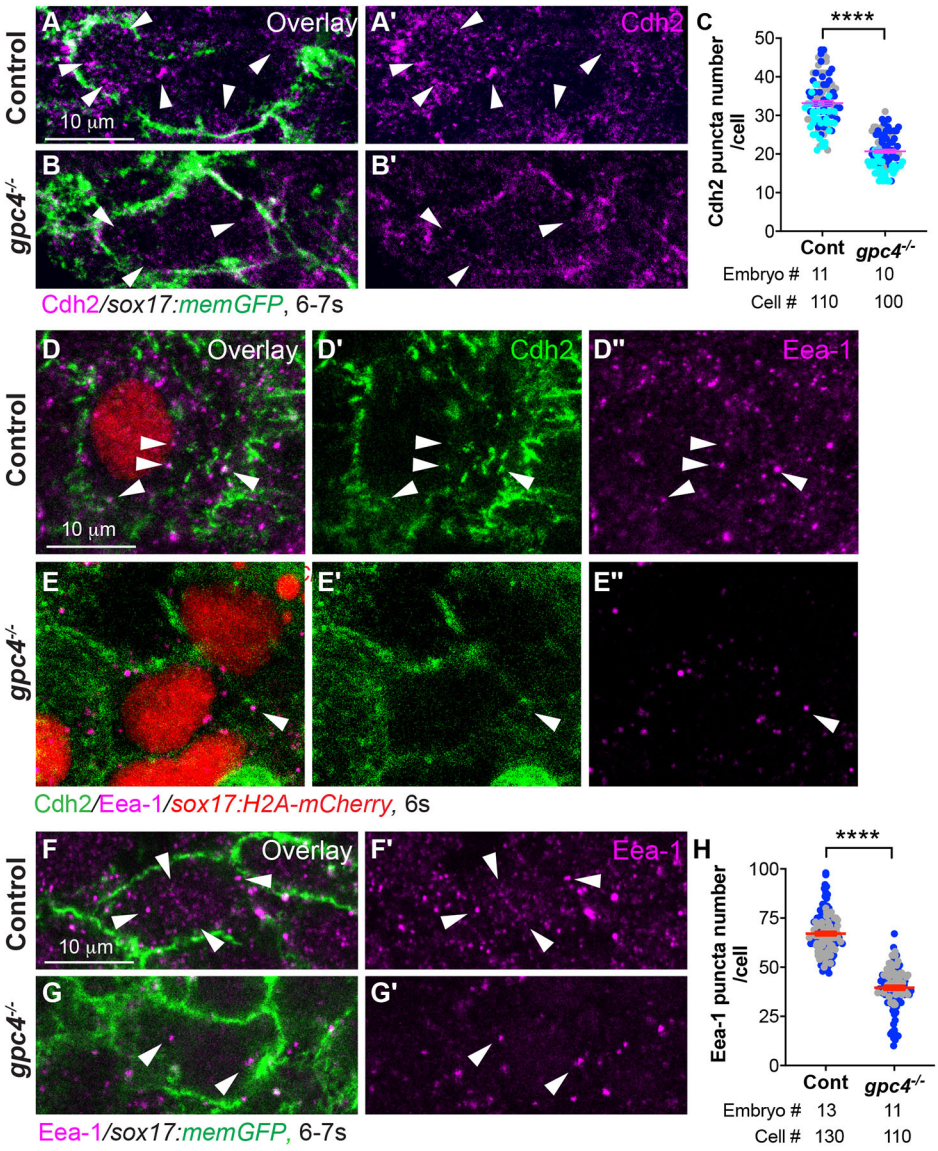

Fig. 6. Cdh2 endocytosis of endodermal cells is impaired in *gpc4*$^{-/-}$ embryos. (A-B′) Confocal images of *Z*-projections of the indicated embryos (high magnification and resolution) showing Cdh2 expression in endodermal cells, as detected by immunofluorescence. Arrowheads indicate cytoplasmic Cdh2-expressing puncta. (C) Average number of cytoplasmic Cdh2 puncta per cell in the indicated embryos from three experiments, represented by different colors. (D-E″) Confocal images of *Z*-projections showing the expression of Cdh2 and Eea-1 (detected by immunofluorescence) in endodermal cells from the indicated embryos. White arrowheads indicate Cdh2 and Eea-1 colocalized puncta. (F-G′) Single *z*-plane confocal images showing Eea-1 expression (detected by immunofluorescence) in endodermal cells from the indicated embryos. White arrowheads indicate Eea-1 expression. (H) Average number of cytoplasmic Eea-1-expressing puncta per cell in the indicated embryos from two separate experiments, represented by different colors. Data are mean±s.e.m. ****P<0.0001 (unpaired, two-tailed Student's *t*-test).

RN-tre resulted in wider endodermal width and impaired polarity of endodermal cells (Fig. S9), suggesting that disrupting Rab5-mediated endocytosis impairs endodermal cell polarity and endoderm C&E.

To investigate the mechanisms by which Gpc4 regulates endocytosis, we examined *rab5c* expression by quantitative real-time (qRT)-PCR and found that it was reduced by 50% in *gpc4*$^{-/-}$ embryos (Fig. 7A). Thus, impaired Cdh2 endocytosis in *gpc4*$^{-/-}$ embryos could be due to decreased Rab5c expression. Therefore, we increased Rab5c activity by injecting mRNA encoding a constitutively active *rab5c*(*CA-rab5c-YFP*) (Ulrich et al., 2005) into embryos obtained from incrossing *gpc4*$^{+/-}$/*Tg(sox17:memCherry)* fish. As expected, overexpression of CA-Rab5c-YFP significantly reduced Cdh2 protein expression on the cell surface of both mesoderm and endoderm cells in *gpc4*$^{-/-}$ embryos (Fig. 7B-D; not shown; P<0.0001; unpaired, two-tailed Student's *t*-test). Examining endodermal cell shape revealed that, although expression of CA-Rab5c-YFP did not cause obvious endoderm defects in control embryos, it significantly rescued the polarity defects of endodermal cells in *gpc4*$^{-/-}$ embryos (Fig. 7E-I; P<0.0001; unpaired, two-tailed Student's *t*-test), which could be a result of reduced expression of Cdh2.

To further test whether Rab5c regulates endodermal cell polarity in a cell-autonomous fashion, we transplanted *gpc4*$^{-/-}$ donor cells expressing CA-rab5c-YFP into control and *gpc4*$^{-/-}$ embryos. Analysis of cell shape revealed that expression of CA-Rab5c in *gpc4*$^{-/-}$ endodermal cells significantly alleviated their polarity defects in hosts of either genotype (Fig. S8D-F; P<0.0001; unpaired, two-tailed Student's *t*-test). In addition, we transplanted WT donor cells expressing RN-Tre into WT host embryos. Expression of RN-Tre should disrupt Rab5-mediated endocytosis, which could lead to an increase in N-cadherin expression and impaired cell polarity. As expected, we found these donor cells displayed rounder cell morphology (Fig. S8G,H), suggesting that the effects of Rab5-mediated endocytosis on endoderm are cell autonomous. Together, these data indicate that Rab5c functions downstream of Gpc4 to regulate plasma membrane levels of Cdh2 in endodermal cells. Thus, Gpc4 promotes endodermal cell polarity, in part, by modulating Rab5c-mediated endocytosis, which regulates the distribution of Cdh2 (Fig. 7J).

DISCUSSION

In this study, we show that, during endoderm C&E at the TB to 12s stages, Gpc4 is required for planar polarity and ML intercalation of endodermal cells. Notably, Cdh2 endocytosis was impaired in *gpc4*-deficient endodermal cells, increasing its expression on the

Development (2021) 148, dev199421. doi:10.1242/dev.199421

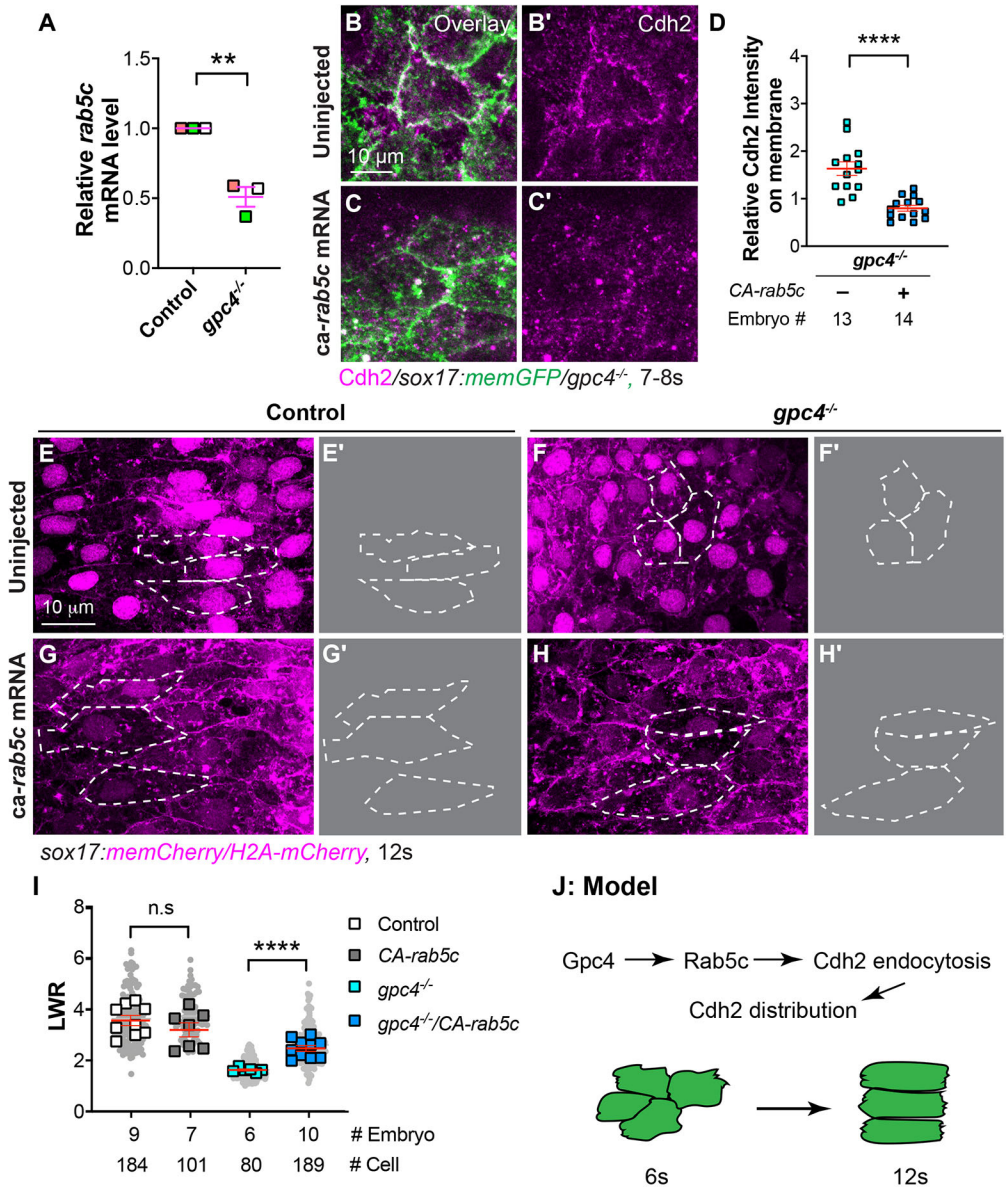

Fig. 7. Overexpression of constitutively active *rab5c* partially rescues defective polarity of endodermal cells in *gpc4*$^{-/-}$ embryos. (A) Relative mRNA levels of *rab5c* compared with *elf1a* in indicated embryos at the 6s stage, as determined by qRT-PCR ***P*<0.01 (unpaired, two-tailed Student's *t*-test from three independent experiments, indicated by different colors). (B-C′) Confocal images (*Z*-projections) showing Cdh2 expression (magenta, detected by immunostaining) of endodermal cells at the 7s-8s stage. (D) Relative fluorescence intensity of Cdh2 expression on the plasma membrane of endodermal cells from embryos in B-C′. (E,F,G,H) Confocal images (*Z*-projections) showing endodermal cells at the 12s stage. (E′,F′,G′,H′) Outlines of some endodermal cells in E,F,G,H (dashed white lines). (I) Average LWR of embryos in E,F,G,H, with the number of cells and embryos analyzed shown. (J) Model illustrating the mechanism through which Gpc4 controls planar cell polarity of endoderm cells. Data are mean±s.e.m. n.s., not significant, **P*>0.05; ***P*<0.01, *****P*<0.0001 (unpaired, two-tailed Student's *t*-test).

plasma membrane. Reducing Cdh2 expression or overexpressing constitutively active Rab5c suppressed polarity defects in *gpc4*-deficient endodermal cells. Collectively, these findings indicate that Gpc4 is required for PCP of endodermal cells during endoderm C&E by partially regulating the distribution of Cdh2 through Rab5c-mediated endocytosis.

Wnt/PCP signaling is required for zebrafish endoderm C&E at a specific developmental stage

During embryogenesis, all germ layers, including endoderm, undergo C&E to establish the body plan. Wnt/PCP signaling is a key pathway that regulates mesoderm C&E (Williams and Solnica-Krezel, 2020). Although Wnt/PCP signaling is implicated in mouse endoderm C&E at gastrulation and gut formation in mouse and *Xenopus*, there is no evidence to support its involvement in the migration of endodermal cells at gastrulation in zebrafish (Mizoguchi et al., 2008). Our current study extends findings from an earlier report (Miles et al., 2017) showing that gut endoderm C&E at segmentation is impaired in *gpc4* mutants, suggesting that Gpc4 is required for this process. However, the previous work did not detect polarity in endodermal cells, suggesting that the endoderm does not move actively but is pulled along by neighboring mesodermal cells during C&E (Miles et al., 2017).

Using a recently created transgenic zebrafish line, we obtained live and static high-resolution images of endodermal cells and discovered that, during C&E, these cells undergo a series of morphogenetic changes at different developmental stages: at the TB to 12s stage, cells polarize increasingly along the ML axis, whereas, after the 12s stage, they undergo apical constriction to facilitate gut-tube formation. The differences between previous work (Miles et al., 2017) and our findings can be attributed to the transgenic lines used and stages analyzed. The *Tg(sox17:EGFP)* line used previously labels the cytosol rather than the cell membrane of endodermal cells with GFP, making cell boundaries difficult to visualize. Furthermore, the endoderm was previously analyzed at the 3s and 16s stages. In our observations, endoderm cells did not exhibit obvious polarity at the 3s stage and displayed apical constriction at the 16s stage. Importantly, we found that GFP-Vangl2 became localized to the anterior edge of polarized endodermal cells, indicating that endodermal cells exhibit planar

Development (2021) 148, dev199421. doi:10.1242/dev.199421

cell polarity. Furthermore, endoderm C&E is impaired in both *vangl2* and *gpc4* mutants (Miles et al., 2017), and we found that cell polarity was lost and GFP-Vangl2 localization was randomized in *gpc4*-deficient endodermal cells. Thus, C&E in both mesoderm and endoderm require Wnt/PCP signaling, which can be regulated by Gpc4.

In zebrafish, the time at which Wnt/PCP signaling is required differs between the mesoderm and endoderm. In mesoderm, Wnt/PCP signaling is required at late gastrulation (Solnica-Krezel and Sepich, 2012), whereas, in endoderm, it is only needed between the TB and 12s stage. Notably, in *gpc4* mutants, endodermal cells retained the ability to undergo apical constriction after the 12s stage; however, because of impaired C&E, the endoderm develops multiple apical focus points, forming an enlarged gut with disconnected lumen. Thus, Wnt/PCP signaling is required for endoderm morphogenesis at the TB and 12s stage, suggesting that this signaling pathway regulates endoderm and mesoderm through different mechanisms.

Gpc4 is required for efficient intercalation of endodermal cells during endoderm C&E

Our live imaging revealed that endoderm C&E is driven by intercalation of endodermal cells, similar to that seen with other cell types. Two major cellular mechanisms drive cell intercalation. One is referred to as 'cell crawling', in which cells extend polarized cellular protrusions that then contact neighboring cells and generate traction between cells to facilitate intercalation. This cellular mechanism was well documented in early studies of gastrulating mesodermal cells in *Xenopus* (Keller, 2002; Keller et al., 2000). However, some epithelial-like cells use another mechanism, so-called 'junctional shrinking', in which cells form strong cell-cell adhesions and engage in junctional remodeling, leading to contraction and expansion of cell junctions along different body axes (Bertet et al., 2004; Blankenship et al., 2006). Recent studies indicate that both mechanisms can occur in the same cells (Shindo and Wallingford, 2014). For example, in neural epithelial cells, both cellular mechanisms are present, but they operate at the apical and basal side of cells, respectively (Williams et al., 2014).

Similarly, our live imaging showed that, during endoderm C&E, endodermal cells display both ML polarized cellular protrusions and cell junction remodeling. However, we found that cell protrusions and junctions were present in different locations in the cell. Notably, some protrusions extended into the ML junctions but were located in different *z*-planes, and extension of protrusions and shortening of junctions were not synchronized. Thus, although cellular protrusions might have influences on junctional changes, they might not directly cause junctional shortening. Our results suggest that these two cellular mechanisms act in concert in endodermal cells, which is consistent with the 'hybrid cell crawling and junction-shrinking model' (Huebner and Wallingford, 2018).

In *gpc4*$^{-/-}$ embryos, endodermal cells failed to elongate and form polarized cellular protrusions, and exhibited impaired junctional changes, which could interfere with efficient intercalation during endoderm C&E. In addition, *gpc4*-deficient endodermal cells tended to form more long-lived rosettes, which likely disrupts the formation of the single lumen in the gut-tube at late segmentation. Although the underlying mechanism for rosette formation is not clear, we speculate that the increase in cell-cell adhesion might play a role. Thus, Gpc4 is necessary for limiting Cdh2 expression and preventing excessive rosette formation, a role that has not been reported previously.

Gpc4 influences endodermal cell polarity by regulating endocytosis of Cdh2

Gastrulating mesodermal cells in *gpc4*$^{-/-}$ embryos display increased cell-cell adhesion (Dohn et al., 2013). Yet, how Gpc4 regulates the polarity of mesoderm cell remains unclear. In this study, we found that, in *gpc4*$^{-/-}$ embryos, Cdh2 expression on the cell membrane of endodermal cells is increased, which contributes to the polarity defects, suggesting that endodermal cell polarity requires appropriate expression of Cdh2. Similar requirement for Cdh2 expression in polarizing cells has been reported in other cell types, including neuronal precursors in mouse, and neural plate cells and neural crest cells in *Xenopus* and zebrafish (Hong and Brewster, 2006; Luccardini et al., 2013; Theveneau et al., 2010).

Cell-cell intercalation requires precise temporal control of junctions because cells must change their relative positions (Walck-Shannon and Hardin, 2014). In addition, junctional changes rely on cell surface adhesion molecules that anchor myosin-mediated contractile proteins (Heisenberg and Bellaiche, 2013; Levayer and Lecuit, 2012). However, we found that, in *cdh2*$^{-/-}$ embryos, the cell shape and C&E of endodermal cells were normal, suggesting that Cdh2 is dispensable for endoderm C&E. It is also possible that, in *cdh2*$^{-/-}$ embryos, expression of other cell-cell adhesion molecules (i.e. *cdh1* in the endoderm) could play a role in regulating endoderm C&E.

Notably, our findings showed that Gpc4 facilitates planar polarization of endodermal cells by regulating the distribution of Cdh2 through Rab5c-mediated endocytosis. However, although our study showed that expression of *rab5c* is reduced in the absence of *gpc4*, the mechanisms by which this occurs are unclear. Nevertheless, Wnt/PCP signaling has been implicated in cadherin trafficking (Ulrich et al., 2005; Warrington et al., 2013). In particular, cadherin assembly and function require the coordination of Rho GTPases, such as RhoA and Rac, which are downstream of the Wnt/PCP signaling pathway (Ratheesh et al., 2013). Therefore, our results are in line with other studies demonstrating that Wnt/PCP signaling regulates cadherin function.

In conclusion, our study provides a detailed analysis of the cell behaviors that underlie endoderm C&E during segmentation and highlight the cell-autonomous role of Gpc4 in the endoderm. We also report original insights into a novel mechanism by which Gpc4 regulates Rab5c-mediated Cdh2 endocytosis and polarized cell behaviors of endoderm. Understanding the mechanisms by which Gpc4 is involved in cadherin trafficking will be an important direction to pursue in order to understand the molecular actions of Gpc4. Ultimately, our study contributes to our understanding of human diseases associated with mutations in *gpc4* and other genes in the Wnt/PCP signaling pathway during development.

MATERIALS AND METHODS

Zebrafish strains and maintenance

Zebrafish were maintained as described previously (Xu et al., 2014). Animal protocols were approved by the University of Iowa Animal Care and Use Committee. Embryos were obtained by natural spawning and staged according to morphological criteria or hours post fertilization (hpf) at 28°C or 32°C, as described previously (Kimmel et al., 1995). Embryos fixed at the 6s and 12s stages were incubated at 28.5°C until 50% epiboly and then at 25°C until the desired developmental stages were reached. The following zebrafish lines were used: AB*/Tuebingen, *Tg(sox17:EGFP)* (Mizoguchi et al., 2008), *Tg(sox17:memCherry)* (Ye et al., 2015), *Tg(sox17:memGFP/H2A-mCherry)* (Hu et al., 2020 preprint), *Tg(vangl2:GFP-Vangl2)* (Sittaramane et al., 2013), *gpc4/knypek*^{fr6} (Topczewski et al., 2001) and *cdh2*^{tm101} (Lele et al., 2002). The *gpc4* mutant was genotyped using a previously published method (Hu et al., 2018). To genotype *cdh2*

Development (2021) 148, dev199421. doi:10.1242/dev.199421

mutant embryos, genomic DNAs were amplified using the following primers: forward, 5′-CCGTATCCATCCGCGTCAT-3′; reverse, 5′-GATGTGTTTTCTTTAATACCTAATAGTCTGCTGAAT-3′. PCR amplicons were distinguished by enzymatic digestion with Apo1: WT DNAs produced one band at 170 bp; mutant DNAs produced two bands at 133 bp and 37 bp.

Generation of transgenic lines

Tg(sox17:GFP-vangl2) was generated using a Tol2-based Multisite Gateway system (Invitrogen) (Kwan et al., 2007; Villefranc et al., 2007) as described previously (Ye et al., 2015) using the following constructs: *pME-GFP-vangl2* (Sittaramane et al., 2013), a 5′-entry vector (*p5E-sox17*), a 3′-entry vector (*p3E*-polyA) and the destination vector *pDestTol2pA2*. Transgenic lines were established using standard techniques as described previously (Xu et al., 2014). The founders were bred to generate multiple stable lines. We used a line that expressed GFP-vangl2 at a modest level and in which embryogenesis was normal. For genotyping of *Tg(sox17:GFP-vang2)*, the following primers were used to generate an amplicon of 413 bp: forward, 5′-CACAACATCGAGGACGGCAG-3′, which targets the open frame sequences of GFP; reverse, 5′-ATCATCCCGATCATCTCCGC3′, which targets the sequence on exon1 in zebrafish *vangl2*.

RNA and morpholino injections

mRNA and MOs were injected into embryos at the one-cell stage at the doses indicated. Capped mRNAs were synthesized using the mMessage mMachine kit (Ambion). RNAs encoding the following genes were used: *sox32* (200 pg), *H2B-GFP* (50 pg), *H2B-RFP* (50 pg), *cdh2-GFP* (100 pg) (Julich et al., 2015), *Rab5c-YFP* (50 pg), *CA-rab5c-YFP* (100 pg) and RN-*tre* (100 pg) (Scholpp and Brand, 2004). The previously validated MO targeting *cdh2* (5′-TCTGTATAAAGAAACCGATAGAGTT-3′) (Lele et al., 2002) was purchased from Gene Tools. The MO was co-injected with the *p53* MO to inhibit potential p53-dependent cell death induced by off-target MO effects (Robu et al., 2007).

Immunofluorescence and western blotting

For immunofluorescence, embryos at different developmental stages were fixed in 2% paraformaldehyde [PFA; in PBS (Research Products International)] for 2 h or overnight at 25°C, washed in PBS, manually deyolked and refixed in 4% PFA for 2 h at 25°C. The embryos were incubated in blocking buffer [PBS with 0.5% bovine serum albumin (BSA) (Research Products International), 0.5% fetal bovine serum (FBS) (Thermo Fisher Scientific), 2% DMSO (Fisher Chemical) and 0.1% Triton (Fisher Scientific)] at 25°C for 1 h and were then incubated with primary antibody in blocking buffer at 4°C overnight. After washing with PBST-DMSO buffer (PBS, 0.1% Triton, 2% DMSO), the embryos were incubated with secondary antibodies in blocking buffer at 25°C for 4 h (Ye and Lin, 2013). Embryos were then mounted in propyl-gallate mounting medium [90% glycerol/PBS with 0.2% *N*-propyl gallate (Sigma-Aldrich)] for confocal imaging. The following antibodies were used: anti-N-cadherin (ab211126, Abcam, 1:200), anti-Eea-1 (ab2900, Abcam, 1:300), Alexa Fluor Plus 647-conjugated goat anti-rabbit secondary antibody (A32733, Thermo Fisher Scientific, 1:200) and Alexa Fluor 568-conjugated goat anti-rabbit secondary antibody (A-11036, Thermo Fisher Scientific, 1:200). Invitrogen Alexa Fluor 568 Phalloidin (A12380, Thermo Fisher Scientific, 1:100) was used to stain F-actin.

For western blotting, protein from zebrafish embryos was collected as previously described (Hu et al., 2018; Link, 2006). Briefly, embryos were deyolked and lysed in 2× SDS loading buffer [2 µl per embryo (Research Products International)]. Equivalent amounts of protein for each sample were loaded onto an SDS-PAGE gel (Research Products International) and protein signals were detected by an Amersham imager 600 detection system (GE Healthcare). The following antibodies were used for immunoblotting: anti-N-cadherin (ab211126, Abcam, 1:2000) and mouse anti-αTubulin (SC-8035, Santa Cruz Biotechnology, 1:2500).

Quantitative real-time PCR

RNAs were isolated from zebrafish embryos using the TRIzol-chloroform method and their cDNAs were synthesized using an iScript Reverse Transcription kit (Bio-Rad) and analyzed by qRT-PCR using the iQ SYBR Green Supermix (Bio-Rad). The following primers were used to amply *cdh2* (forward, 5′-GCCATGTCAGCCTGGTTTC-3′; reverse, 5′-TCCCATC-GGCGTCTATCC-3′) and *rab5c* (forward, 5′-GCACCATTGGAGCT-GCTTTC-3′; reverse, 5′-ATGTCGTAGACGACGATGGC-3′).

Endoderm transplantation

Endoderm transplantation was performed as previously described (Ye and Lin, 2013). Briefly, donor embryos were injected with *sox32* mRNA (conferring an endodermal identity to all cells) together with *H2B-GFP* or *H2B-RFP* mRNA or 1% rhodamine dextran (70,000 MW, lysine fixable, Thermo Fisher Scientific), which were used as lineage tracers. Embryos were incubated at 28°C until the ‘High stage’ (3.33 hpf). Then, 20-30 cells were transplanted from donors into host embryos at the blastoderm margin. At the 11s-12s stage, host embryos were screened for donor cells in the posterior endoderm region before confocal imaging.

Microscopy and time-lapse imaging

For still epifluorescence images, fixed embryos were mounted in 2.5% methylcellulose and imaged using a Leica DMI 6000 microscope with a 5×/NA 0.15 objective. Bright-field images were taken on a Leica M165FC stereomicroscope with a Leica DFC290 Color Digital Camera. Confocal imaging was performed on Zeiss inverted LSM880 or LSM700 laser scanning confocal microscopes. For still confocal images, the head and tail regions of the deyolked embryos were removed and the part of the embryo containing the posterior endoderm was used to prepare flat mount samples. *z*-stack images were obtained using LD C-Apochromat 20×/NA 0.8, EC Plan-Neofluar 40×/NA 1.3 oil or LD C-Apochromat 40×/NA 1.1 water objectives. The following imaging parameters were used for collective confocal images: 1024×1024 pixels, 8 speed, 2 averaging.

For time-lapse movies, embryos were embedded in low melting agarose gel (1%) (Research Products International) using glass-bottom dishes (Cellvis) as described previously (Hu et al., 2018). Images were taken on a Zeiss inverted LSM880 scope. For Movies 1 and 4, the posterior region of endoderm was focused and images were acquired using an LD C-Apochromat 20×/NA 0.8 objective and the Fast Airy-scan module at 1 µm *z*-intervals, 5 min intervals. Endoderm cells in the posterior region of embryos were focused and readjusted as necessary throughout imaging. To determine protrusive behaviors of the cells (Movies 2, 4), an LD C-Apochromat 40×/NA 1.1 water objective was used at 1 µm *z*-intervals every 15 s. To analyze cellular protrusions in endoderm mosaically labeled with different fluorescent proteins, cells from *Tg(sox17:H2A-Cherry)* donor embryos injected with *sox32* and *memGFP* mRNAs were transplanted into *Tg(sox17:memCherry/H2A-Cherry)* embryos. At the 5s-6s stage, host embryos were screened for donor cells in the posterior endoderm region before confocal imaging. Time-lapse imaging was performed using an LD C-Apochromat 40×/NA 1.1 water objective with 1.5 zoom at 2 µm *z*-intervals every 30 s.

Image analysis

Confocal images were acquired using the same setting for all embryos in each experiment. All images were processed using Fiji software (ImageJ), and edited and compiled using Adobe Photoshop and Adobe Illustrator.

Analysis of cell morphology

z-stack images were obtained as described above and rotated to position embryos with correct AP and ML axis orientation. Endodermal cells of interest were outlined using the ‘Polygon’ and region of interest (ROI) manager tools from Fiji. Data were exported to Microsoft Excel and the LWR as well as the angle of the long axes of endodermal cells with respect to the ML axis were measured as previously described (Topczewski et al., 2001). The angles were exported to the Past3 software and rose diagrams were generated.

Analysis of cell behaviors underlying endoderm C&E

Confocal time-lapse movies acquired at a 20× objective were analyzed for movements of endodermal cells at the 7s-12s stage. The junctional changes at

Development (2021) 148, dev199421. doi:10.1242/dev.199421

5-min intervals over the entire time-lapse were manually tracked (Chomczynski and Mackey, 1995). The following parameters were assessed: (1) the number of ML junctions (T3) in every 100 endodermal cells; (2) the rate at which the T3 junction was shrinking (the length of T3 junctions divided by the time required for them contracting to T2); and (3) the efficiency of separating one pair of cells (i.e. assessment of whether junctions were completed and the changes from T3 to T1 to separate a pair of cells along a perpendicular axis). In addition, we tracked the number of newly formed rosettes and total number of rosettes over the time-lapse period.

Analysis of cellular protrusions

Confocal time-lapse movies acquired at a 40× water objective were analyzed to determine the orientation of cell protrusions. Using Fiji software, a line was drawn from the base to tip of the cell protrusion to determine the orientation. Data were saved as ROI files and exported to Microsoft Excel to obtain angles of cell protrusions; Past3 software was used to generate rose diagrams depicting their orientation.

Analysis of Cdh2 expression

To quantify the intensity of the Cdh2 signal, maximum *Z*-projection images were obtained from ∼5 µm *z*-planes to cover only endoderm cells and converted into 32-bit images using Fiji software. The lower and upper thresholds were set to 0 and 80, respectively and the background was set to NaN. The Polygon tool was used to select a small region of plasma membrane of endodermal cells as the ROI. At least ten endodermal cells from each embryo were analyzed. The mean intensity of Cdh2 signal from each ROI was exported to Microsoft Excel. The average of the mean intensity from control and mutant embryos, as well as the fold change in intensity, were calculated as the relative intensity of mutant versus sibling embryos in each biological replicate.

Analyses of GFP-Vangl2 distribution in endodermal cells

To quantify the distribution of GFP-Vangl2 signal, maximum *Z*-projection images were obtained and converted into 32-bit images using Fiji software. The lower and upper thresholds were set to 5 and 50, respectively and the background was set to NaN. The Polygon tool was used to select a small ROI of plasma membrane on the ML and AP boundaries of endodermal cells. The maximum intensity of the ROI on ML and AP boundaries from each embryo were measured.

Analysis of cytoplasmic puncta

High-magnification (63× oil objective) confocal images were used to analyze the cytoplasmic punta. A small region of endoderm was chosen and maximum *Z*-projection images were obtained from *z*-planes to cover only endoderm cells. The number of cytoplasmic vesicles expressing Cdh2 or Eea-1 in the endodermal cells was counted. At least ten endodermal cells from each embryo were analyzed.

Statistical analysis

Data were compiled from different clusters of embryos in two to three biological replicates and presented as the mean±s.e.m. Statistical analyses were performed using the unpaired Student's two-tailed *t*-test with unequal variance or one-way ANOVA followed by a Tukey's multiple comparisons test, using the Prism software (GraphPad). $P<0.05$ was considered as significant. The numbers of cells and embryos analyzed in each experiment are indicated in the figures and/or figure legends.

Acknowledgements

We are grateful to Dr Lilianna Solnica-Krezel (Washington University), Anand Chandraskhar (University of Missouri), Jason R. Jessen (Middle Tennessee State University) and Dorthe Julich (Yale University) for providing the plasmid constructs and transgenic zebrafish lines. We thank other members in the laboratories of Drs Lin and Robert Cornell (University of Iowa), as well as Lilianna Solnica-Krezel and Diane Sepich (Washington University in St Louis) for their helpful discussions and suggestions. We also thank Matthew Culver for excellent fish care and technical support.

Competing interests

The authors declare no competing or financial interests.

Author contributions

Conceptualization: A.K.B., B.H., F.L.; Methodology: A.K.B., B.H., J.J.R., M.M.; Validation: A.K.B.; Formal analysis: A.K.B., J.J.R., M.M., F.L.; Investigation: A.K.B., J.J.R.; Data curation: A.K.B., B.H., F.L.; Writing - original draft: A.K.B., F.L.; Writing - review & editing: F.L.; Visualization: A.K.B., J.J.R.; Supervision: F.L.; Project administration: F.L.; Funding acquisition: F.L.

Funding

This work was supported by funding to F.L. from National Institutes of Health (1R56DK123610-01). Deposited in PMC for release after 12 months.

Peer review history

The peer review history is available online at https://journals.biologists.com/dev/article-lookup/doi/10.1242/dev.199421

References

Bertet, C., Sulak, L. and Lecuit, T. (2004). Myosin-dependent junction remodelling controls planar cell intercalation and axis elongation. *Nature* **429**, 667-671. doi:10.1038/nature02590

Blankenship, J. T., Backovic, S. T., Sanny, J. S. P., Weitz, O. and Zallen, J. A. (2006). Multicellular rosette formation links planar cell polarity to tissue morphogenesis. *Dev. Cell* **11**, 459-470. doi:10.1016/j.devcel.2006.09.007

Butler, M. T. and Wallingford, J. B. (2017). Planar cell polarity in development and disease. *Nat. Rev. Mol. Cell Biol.* **18**, 375-388. doi:10.1038/nrm.2017.11

Camand, E., Peglion, F., Osmani, N., Sanson, M. and Etienne-Manneville, S. (2012). N-cadherin expression level modulates integrin-mediated polarity and strongly impacts on the speed and directionality of glial cell migration. *J. Cell Sci.* **125**, 844-857. doi:10.1242/jcs.087668

Cervantes, S., Yamaguchi, T. P. and Hebrok, M. (2009). Wnt5a is essential for intestinal elongation in mice. *Dev. Biol.* **326**, 285-294. doi:10.1016/j.ydbio.2008.11.020

Chomczynski, P. and Mackey, K. (1995). Short technical reports. Modification of the TRI reagent procedure for isolation of RNA from polysaccharide- and proteoglycan-rich sources. *Biotechniques* **19**, 942-945.

Ciruna, B., Jenny, A., Lee, D., Mlodzik, M. and Schier, A. F. (2006). Planar cell polarity signalling couples cell division and morphogenesis during neurulation. *Nature* **439**, 220-224. doi:10.1038/nature04375

D'Souza-Schorey, C. (2005). Disassembling adherens junctions: breaking up is hard to do. *Trends Cell Biol.* **15**, 19-26. doi:10.1016/j.tcb.2004.11.002

Detrick, R. J., Dickey, D. and Kintner, C. R. (1990). The effects of N-cadherin misexpression on morphogenesis in Xenopus embryos. *Neuron* **4**, 493-506. doi:10.1016/0896-6273(90)90108-R

Dohn, M. R., Mundell, N. A., Sawyer, L. M., Dunlap, J. A. and Jessen, J. R. (2013). Planar cell polarity proteins differentially regulate extracellular matrix organization and assembly during zebrafish gastrulation. *Dev. Biol.* **383**, 39-51. doi:10.1016/j.ydbio.2013.08.027

Dush, M. K. and Nascone-Yoder, N. M. (2013). Jun N-terminal kinase maintains tissue integrity during cell rearrangement in the gut. *Development* **140**, 1457-1466. doi:10.1242/dev.086850

Garcia-Garcia, M. J., Shibata, M. and Anderson, K. V. (2008). Chato, a KRAB zinc-finger protein, regulates convergent extension in the mouse embryo. *Development* **135**, 3053-3062. doi:10.1242/dev.022897

Heisenberg, C.-P. and Bellaïche, Y. (2013). Forces in tissue morphogenesis and patterning. *Cell* **153**, 948-962. doi:10.1016/j.cell.2013.05.008

Hong, E. and Brewster, R. (2006). N-cadherin is required for the polarized cell behaviors that drive neurulation in the zebrafish. *Development* **133**, 3895-3905. doi:10.1242/dev.02560

Horne-Badovinac, S., Lin, D., Waldron, S., Schwarz, M., Mbamalu, G., Pawson, T., Jan, Y.-N., Stainier, D. Y. R. and Abdelilah-Seyfried, S. (2001). Positional cloning of heart and soul reveals multiple roles for PKCλ in zebrafish organogenesis. *Curr. Biol.* **11**, 1492-1502. doi:10.1016/S0960-9822(01)00458-4

Hu, B., Gao, Y., Davies, L., Woo, S., Topczewski, J., Jessen, J. R. and Lin, F. (2018). Glypican 4 and Mmp14 interact in regulating the migration of anterior endodermal cells by limiting extracellular matrix deposition. *Development* **145**, dev163303. doi:10.1242/dev.163303

Hu, B., Balaraju, A. K., Rodriguez, J. J., Gao, Y., Nguyen, N. T., Steen, H., Suhaib, S., Chen, S. and Lin, F. (2020). Glypican4 mediates Wnt transport between germ layers via signaling filopodia. *bioRxiv*, 2020.2009.2008.288613. doi:10.1101/2020.09.08.288613

Huebner, R. J. and Wallingford, J. B. (2018). Coming to consensus: a unifying model emerges for convergent extension. *Dev. Cell* **46**, 389-396. doi:10.1016/j.devcel.2018.08.003

Jessen, J. R., Topczewski, J., Bingham, S., Sepich, D. S., Marlow, F., Chandrasekhar, A. and Solnica-Krezel, L. (2002). Zebrafish trilobite identifies new roles for Strabismus in gastrulation and neuronal movements. *Nat. Cell Biol.* **4**, 610-615. doi:10.1038/ncb828

Jülich, D., Cobb, G., Melo, A. M., McMillen, P., Lawton, A. K., Mochrie, S. G. J., Rhoades, E. and Holley, S. A. (2015). Cross-scale integrin regulation organizes ECM and tissue topology. *Dev. Cell* **34**, 33-44. doi:10.1016/j.devcel.2015.05.005

Keller, R. (2002). Shaping the vertebrate body plan by polarized embryonic cell movements. *Science* **298**, 1950-1954. doi:10.1126/science.1079478

Keller, R. and Sutherland, A. (2020). Convergent extension in the amphibian, *Xenopus laevis*. *Curr. Top. Dev. Biol.* **136**, 271-317. doi:10.1016/bs.ctdb.2019.11.013

Keller, R., Davidson, L., Edlund, A., Elul, T., Ezin, M., Shook, D. and Skoglund, P. (2000). Mechanisms of convergence and extension by cell intercalation. *Philos. Trans. R. Soc. B Biol. Sci.* **355**, 897-922. doi:10.1098/rstb.2000.0626

Kimmel, C. B., Ballard, W. W., Kimmel, S. R., Ullmann, B. and Schilling, T. F. (1995). Stages of embryonic development of the zebrafish. *Dev. Dyn.* **203**, 253-310. doi:10.1002/aja.1002030302

Kwan, K. M., Fujimoto, E., Grabher, C., Mangum, B. D., Hardy, M. E., Campbell, D. S., Parant, J. M., Yost, H. J., Kanki, J. P. and Chien, C.-B. (2007). The Tol2kit: a multisite gateway-based construction kit for Tol2 transposon transgenesis constructs. *Dev. Dyn.* **236**, 3088-3099. doi:10.1002/dvdy.21343

Lele, Z., Folchert, A., Concha, M., Rauch, G.-J., Geisler, R., Rosa, F., Wilson, S. W., Hammerschmidt, M. and Bally-Cuif, L. (2002). *parachute/n-cadherin* is required for morphogenesis and maintained integrity of the zebrafish neural tube. *Development* **129**, 3281-3294. doi:10.1242/dev.129.14.3281

Levayer, R. and Lecuit, T. (2012). Biomechanical regulation of contractility: spatial control and dynamics. *Trends Cell Biol.* **22**, 61-81. doi:10.1016/j.tcb.2011.10.001

Lindsay, A. J. and McCaffrey, M. W. (2017). Rab coupling protein mediated endosomal recycling of N-cadherin influences cell motility. *Oncotarget* **8**, 104717-104732. doi:10.18632/oncotarget.10513

Link, V., Carvalho, L., Castanon, I., Stockinger, P., Shevchenko, A. and Heisenberg, C.-P. (2006). Identification of regulators of germ layer morphogenesis using proteomics in zebrafish. *J. Cell Sci.* **119**, 2073-2083. doi:10.1242/jcs.02928

Luccardini, C., Hennekinne, L., Viou, L., Yanagida, M., Murakami, F., Kessaris, N., Ma, X., Adelstein, R. S., Mege, R.-M. and Metin, C. (2013). N-cadherin sustains motility and polarity of future cortical interneurons during tangential migration. *J. Neurosci.* **33**, 18149-18160. doi:10.1523/JNEUROSCI.0593-13.2013

Matsuyama, M., Aizawa, S. and Shimono, A. (2009). Sfrp controls apicobasal polarity and oriented cell division in developing gut epithelium. *PLoS Genet.* **5**, e1000427. doi:10.1371/journal.pgen.1000427

Miles, L. B., Mizoguchi, T., Kikuchi, Y. and Verkade, H. (2017). A role for planar cell polarity during early endoderm morphogenesis. *Biol. Open* **6**, 531-539. doi:10.1242/bio.021899

Mizoguchi, T., Verkade, H., Heath, J. K., Kuroiwa, A. and Kikuchi, Y. (2008). Sdf1/Cxcr4 signaling controls the dorsal migration of endodermal cells during zebrafish gastrulation. *Development* **135**, 2521-2529. doi:10.1242/dev.020107

Mu, F. T., Callaghan, J. M., Steele-Mortimer, O., Stenmark, H., Parton, R. G., Campbell, P. L., McCluskey, J., Yeo, J. P., Tock, E. P. and Toh, B. H. (1995). EEA1, an early endosome-associated protein. EEA1 is a conserved α-helical peripheral membrane protein flanked by cysteine "fingers" and contains a calmodulin-binding IQ motif. *J. Biol. Chem.* **270**, 13503-13511. doi:10.1074/jbc.270.22.13503

Nagaoka, T., Ohashi, R., Inutsuka, A., Sakai, S., Fujisawa, N., Yokoyama, M., Huang, Y. H., Igarashi, M. and Kishi, M. (2014). The Wnt/planar cell polarity pathway component Vangl2 induces synapse formation through direct control of N-cadherin. *Cell Rep.* **6**, 916-927. doi:10.1016/j.celrep.2014.01.044

Nair, S. and Schilling, T. F. (2008). Chemokine signaling controls endodermal migration during zebrafish gastrulation. *Science* **322**, 89-92. doi:10.1126/science.1160038

Nishimura, T. and Takeichi, M. (2009). Remodeling of the adherens junctions during morphogenesis. *Curr. Top. Dev. Biol.* **89**, 33-54. doi:10.1016/S0070-2153(09)89002-9

Ober, E. A., Field, H. A. and Stainier, D. Y. R. (2003). From endoderm formation to liver and pancreas development in zebrafish. *Mech. Dev.* **120**, 5-18. doi:10.1016/S0925-4773(02)00327-1

Pézeron, G., Mourrain, P., Courty, S., Ghislain, J., Becker, T. S., Rosa, F. M. and David, N. B. (2008). Live analysis of endodermal layer formation identifies random walk as a novel gastrulation movement. *Curr. Biol.* **18**, 276-281. doi:10.1016/j.cub.2008.01.028

Piloto, S. and Schilling, T. F. (2010). Ovo1 links Wnt signaling with N-cadherin localization during neural crest migration. *Development* **137**, 1981-1990. doi:10.1242/dev.048439

Radice, G. L. (2013). N-cadherin-mediated adhesion and signaling from development to disease: lessons from mice. *Prog. Mol. Biol. Transl. Sci.* **116**, 263-289. doi:10.1016/B978-0-12-394311-8.00012-1

Ratheesh, A., Priya, R. and Yap, A. S. (2013). Coordinating Rho and Rac: the regulation of Rho GTPase signaling and cadherin junctions. *Prog. Mol. Biol. Transl. Sci.* **116**, 49-68. doi:10.1016/B978-0-12-394311-8.00003-0

Reed, R. A., Womble, M. A., Dush, M. K., Tull, R. R., Bloom, S. K., Morckel, A. R., Devlin, E. W. and Nascone-Yoder, N. M. (2009). Morphogenesis of the primitive gut tube is generated by Rho/ROCK/myosin II-mediated endoderm rearrangements. *Dev. Dyn.* **238**, 3111-3125. doi:10.1002/dvdy.22157

Robu, M. E., Larson, J. D., Nasevicius, A., Beiraghi, S., Brenner, C., Farber, S. A. and Ekker, S. C. (2007). p53 activation by knockdown technologies. *PLoS Genet.* **3**, e78. doi:10.1371/journal.pgen.0030078

Roszko, I., Sepich, D. S., Jessen, J. R., Chandrasekhar, A. and Solnica-Krezel, L. (2015). A dynamic intracellular distribution of Vangl2 accompanies cell polarization during zebrafish gastrulation. *Development* **142**, 2508-2520. doi:10.1242/dev.119032

Scholpp, S. and Brand, M. (2004). Endocytosis controls spreading and effective signaling range of Fgf8 protein. *Curr. Biol.* **14**, 1834-1841. doi:10.1016/j.cub.2004.09.084

Sepich, D. S., Usmani, M., Pawlicki, S. and Solnica-Krezel, L. (2011). Wnt/PCP signaling controls intracellular position of MTOCs during gastrulation convergence and extension movements. *Development* **138**, 543-552. doi:10.1242/dev.053959

Shindo, A. and Wallingford, J. B. (2014). PCP and septins compartmentalize cortical actomyosin to direct collective cell movement. *Science* **343**, 649-652. doi:10.1126/science.1243126

Sittaramane, V., Pan, X., Glasco, D. M., Huang, P., Gurung, S., Bock, A., Li, S., Wang, H., Kawakami, K., Matise, M. P. et al. (2013). The PCP protein Vangl2 regulates migration of hindbrain motor neurons by acting in floor plate cells, and independently of cilia function. *Dev. Biol.* **382**, 400-412. doi:10.1016/j.ydbio.2013.08.017

Solnica-Krezel, L. and Sepich, D. S. (2012). Gastrulation: making and shaping germ layers. *Annu. Rev. Cell Dev. Biol.* **28**, 687-717. doi:10.1146/annurev-cellbio-092910-154043

Spence, J. R., Lauf, R. and Shroyer, N. F. (2011). Vertebrate intestinal endoderm development. *Dev. Dyn.* **240**, 501-520. doi:10.1002/dvdy.22540

Theveneau, E., Marchant, L., Kuriyama, S., Gull, M., Moepps, B., Parsons, M. and Mayor, R. (2010). Collective chemotaxis requires contact-dependent cell polarity. *Dev. Cell* **19**, 39-53. doi:10.1016/j.devcel.2010.06.012

Topczewski, J., Sepich, D. S., Myers, D. C., Walker, C., Amores, A., Lele, Z., Hammerschmidt, M., Postlethwait, J. and Solnica-Krezel, L. (2001). The zebrafish glypican knypek controls cell polarity during gastrulation movements of convergent extension. *Dev. Cell* **1**, 251-264. doi:10.1016/S1534-5807(01)00005-3

Ulrich, F., Krieg, M., Schötz, E.-M., Link, V., Castanon, I., Schnabel, V., Taubenberger, A., Mueller, D., Puech, P.-H. and Heisenberg, C.-P. (2005). Wnt11 functions in gastrulation by controlling cell cohesion through Rab5c and E-cadherin. *Dev. Cell* **9**, 555-564. doi:10.1016/j.devcel.2005.08.011

Villefranc, J. A., Amigo, J. and Lawson, N. D. (2007). Gateway compatible vectors for analysis of gene function in the zebrafish. *Dev. Dyn.* **236**, 3077-3087. doi:10.1002/dvdy.21354

Walck-Shannon, E. and Hardin, J. (2014). Cell intercalation from top to bottom. *Nat. Rev. Mol. Cell Biol.* **15**, 34-48. doi:10.1038/nrm3723

Wallace, K. N. and Pack, M. (2003). Unique and conserved aspects of gut development in zebrafish. *Dev. Biol.* **255**, 12-29. doi:10.1016/S0012-1606(02)00034-9

Warga, R. M. and Nusslein-Volhard, C. (1999). Origin and development of the zebrafish endoderm. *Development* **126**, 827-838. doi:10.1242/dev.126.4.827

Warrington, S. J., Strutt, H. and Strutt, D. (2013). The Frizzled-dependent planar polarity pathway locally promotes E-cadherin turnover via recruitment of RhoGEF2. *Development* **140**, 1045-1054. doi:10.1242/dev.088724

Wen, J., Chiang, Y. J., Gao, C., Xue, H., Xu, J., Ning, Y., Hodes, R. J., Gao, X. and Chen, Y.-G. (2010). Loss of Dact1 disrupts planar cell polarity signaling by altering dishevelled activity and leads to posterior malformation in mice. *J. Biol. Chem.* **285**, 11023-11030. doi:10.1074/jbc.M109.085381

Williams, M., Yen, W., Lu, X. and Sutherland, A. (2014). Distinct apical and basolateral mechanisms drive planar cell polarity-dependent convergent extension of the mouse neural plate. *Dev. Cell* **29**, 34-46. doi:10.1016/j.devcel.2014.02.007

Williams, M. L. K. and Solnica-Krezel, L. (2020). Cellular and molecular mechanisms of convergence and extension in zebrafish. *Curr. Top. Dev. Biol.* **136**, 377-407. doi:10.1016/bs.ctdb.2019.08.001

Xu, H., Ye, D., Behra, M., Burgess, S., Chen, S. and Lin, F. (2014). Gβ1 controls collective cell migration by regulating the protrusive activity of leader cells in the posterior lateral line primordium. *Dev. Biol.* **385**, 316-327. doi:10.1016/j.ydbio.2013.10.027

Yamada, M., Udagawa, J., Matsumoto, A., Hashimoto, R., Hatta, T., Nishita, M., Minami, Y. and Otani, H. (2010). Ror2 is required for midgut elongation during mouse development. *Dev. Dyn.* **239**, 941-953. doi:10.1002/dvdy.22212

Ye, D. and Lin, F. (2013). S1pr2/Gα13 signaling controls myocardial migration by regulating endoderm convergence. *Development* **140**, 789-799. doi:10.1242/dev.085340

Ye, D., Xie, H., Hu, B. and Lin, F. (2015). Endoderm convergence controls subduction of the myocardial precursors during heart-tube formation. *Development* **142**, 2928-2940. doi:10.1242/dev.113944

Yin, C., Kiskowski, M., Pouille, P.-A., Farge, E. and Solnica-Krezel, L. (2008). Cooperation of polarized cell intercalations drives convergence and extension of presomitic mesoderm during zebrafish gastrulation. *J. Cell Biol.* **180**, 221-232. doi:10.1083/jcb.200704150

Zerial, M. and McBride, H. (2001). Rab proteins as membrane organizers. *Nat. Rev. Mol. Cell Biol.* **2**, 107-117. doi:10.1038/35052055

Zorn, A. M. and Wells, J. M. (2009). Vertebrate endoderm development and organ formation. *Annu. Rev. Cell Dev. Biol.* **25**, 221-251. doi:10.1146/annurev.cellbio.042308.113344

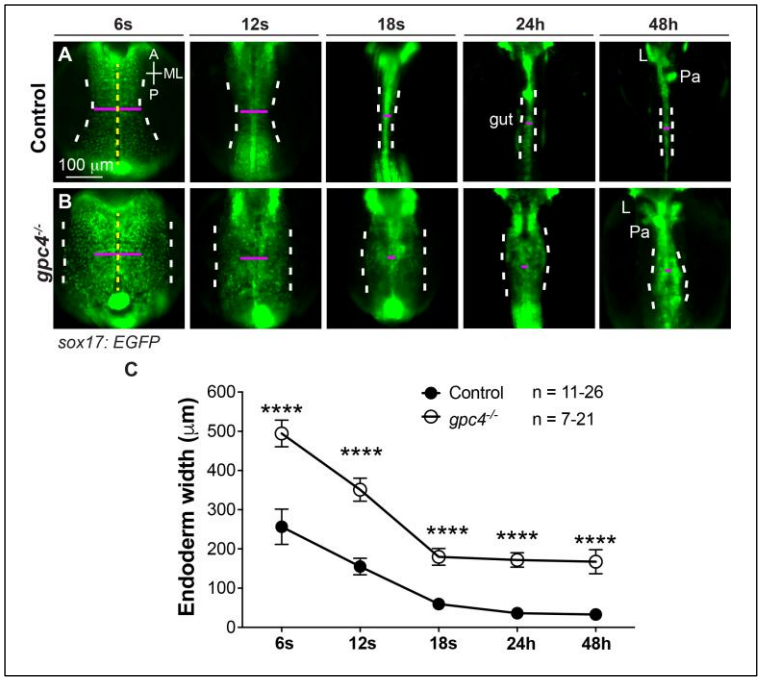

Fig. S1. Gpc4 is required for endoderm morphogenesis during segmentation.
(A-B) Epifluorescence imaging on endoderm in the posterior region of the indicated embryos at different stages. Dashed white lines, endoderm boundary; Magenta lines (equal length in embryos at the same stage), endoderm width; Yellow dashed lines, midline; L, liver; Pa, pancreas; A, anterior; P, posterior; ML, mediolateral. (C) Average endoderm width of embryos shown in A, B. The number of embryos analyzed is indicated. **** P <0.0001, Unpaired two-tailed student's t-test.

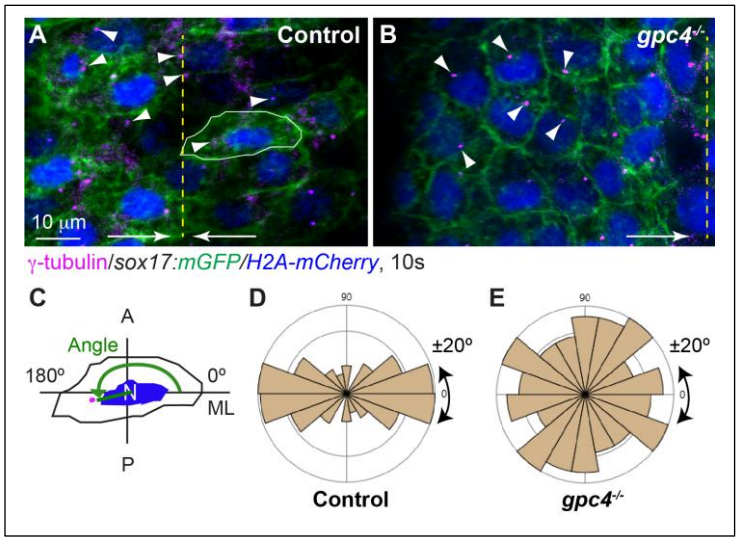

Fig. S2. Positioning of MTOCs in endodermal cells is impaired in *gpc4*$^{-/-}$ embryos.
(A,B) Confocal images (Z-projection) of endodermal cells showing expression of γ-tubulin, which labels microtubule organizing centers (MTOCs, arrowheads, detected by immunostaining) of endodermal cells. Yellow dashed lines, midline; arrows, the directions of endodermal convergence. (C) Schematic depicting how MTOC position is measured relative to the nucleus (N) and the ML axis. The angle measured is indicated by the green line. (D,E) Rose diagrams showing the distribution of the MTOC angle (each bin, 20º) in control embryos (79 cells, 6 embryos) and *gpc4*$^{-/-}$ embryos (90 cells, 5 embryos).

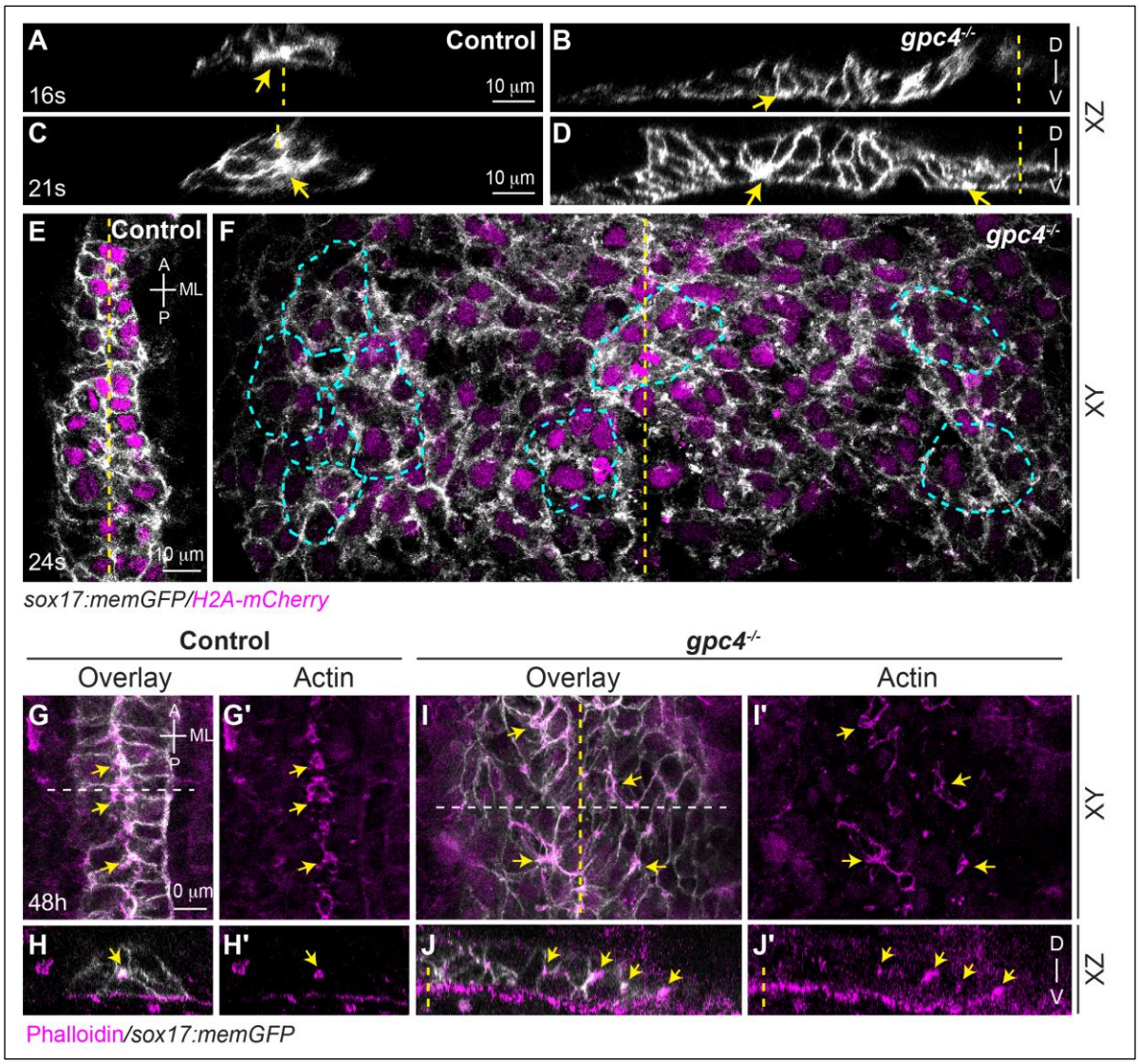

Fig. S3. Endodermal cells change shape during late segmentation.

(A-D) Confocal images (XZ view) of gut-endoderm in the indicated embryos. Only the left side of the endoderm is shown in B, D. Yellow arrows, apical constriction sites. (E-F) Z-projection confocal images (XY view) of the endoderm in the indicated embryos. Cyan dashed lines outline rosettes. (G-J′) Confocal images of gut endoderm in the indicated embryos, showing expression of Actin (detected by Phalloidin staining). (G-I′) Z projection images (XY view). White dashed lines: the region that the XZ cross section was taken. (H-J′) XZ view. Only the right side of the endoderm is shown in J-J′. Yellow arrows: actin enriched sites. Yellow dashed line, midline; D, dorsal; V, ventral; A, anterior; P, posterior; ML, mediolateral.

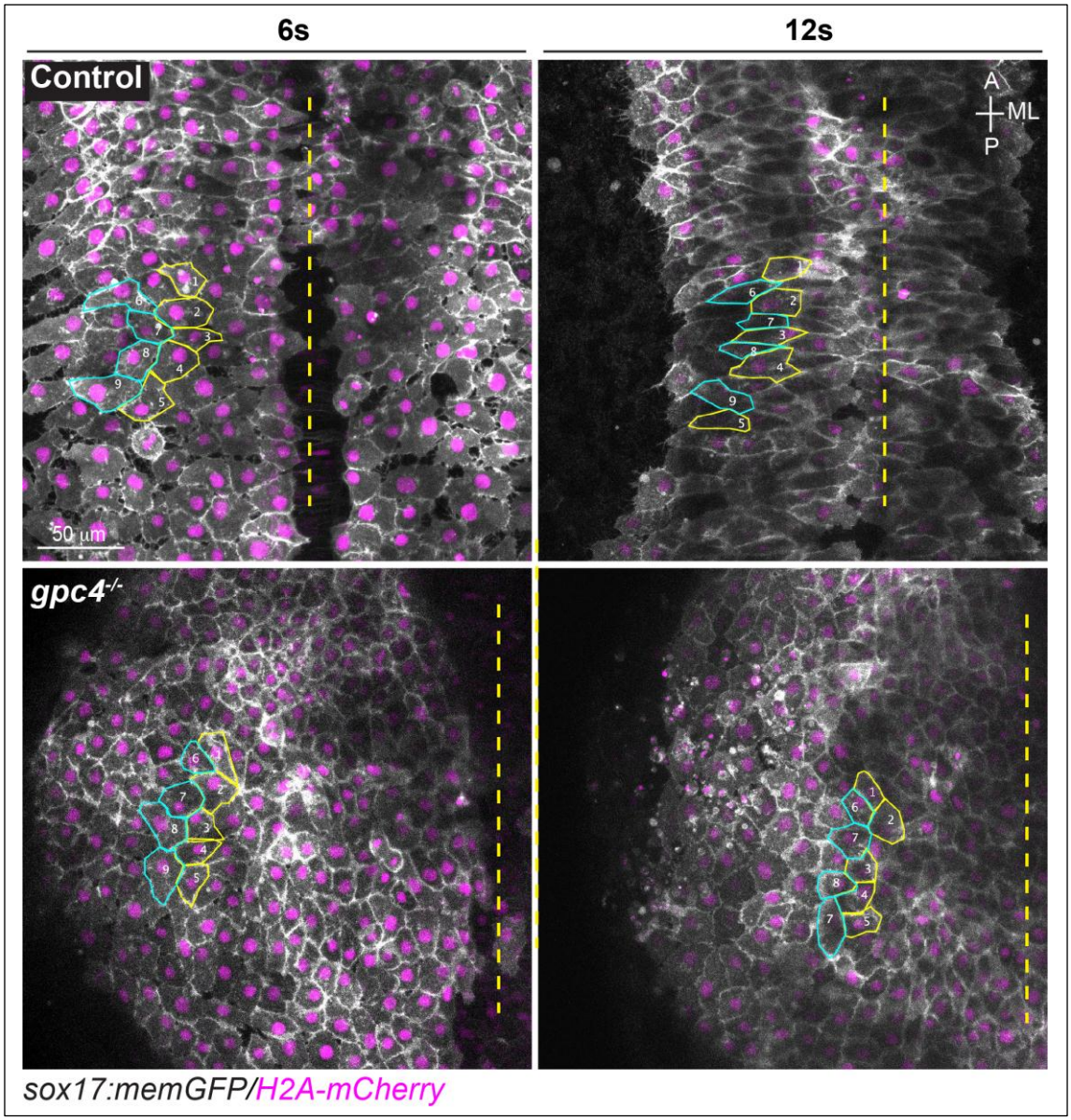

Fig. S4. Gpc4 is required for efficient endoderm convergence.

Snapshots from confocal movies (movie #1 and #3) of the endoderm at the beginning and end of timepoints (6s and 12s) in control and *gpc4*$^{-/-}$ embryos. Selected cells are marked (the same cells are labeled with the same number) to show their relative positions at two different timepoints. Only the left side of the endoderm is shown in *gpc4*$^{-/-}$embryos. Yellow dashed line, midline; A, anterior; P, posterior; ML, mediolateral.

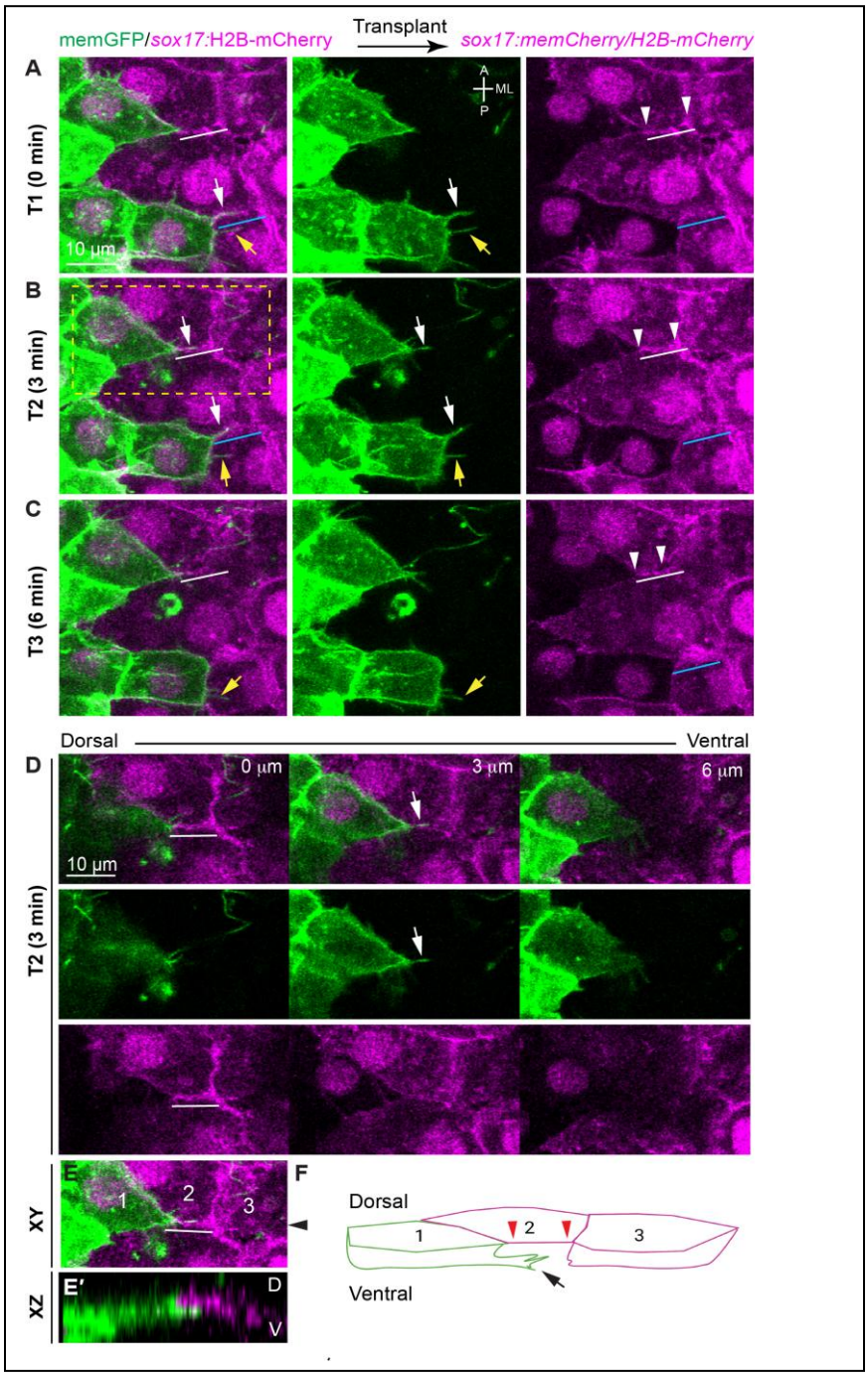

Fig. S5. **Cellular behaviors of endodermal cells during C&E.** Donor cells from *Tg(sox17:H2A-Cherry)* embryos injected with *memGFP* and *sox32* RNAs were transplanted into *Tg(sox17: memCherry/H2A-Cherry)* host embryos. Time-lapse experiments were performed on the host embryos at 6s, at which the endoderm contained memGFP-expressing donor endoderm cells. (A-C) Snapshots of Z-projected

confocal images at different time-points showing the protrusions extended from memGFP-expressing donor endodermal cells and the junctional changes in neighboring memCherry-expressing host endodermal cells. (D) Montage of Z-planes from the dorsal to ventral side of endodermal cells shown in the yellow dashed rectangle box in B. (E) Z-projected confocal image showing a donor cell protrusion into the ML junction of the neighboring endodermal cells, shown in the yellow dashed rectangle box in B. (E′) XZ view of image taken from E in the area indicated by the arrowhead. (F) Diagram depicting a cell protrusion and the shortening ML junction in the neighboring endodermal cells. White arrows, cellular protrusions extended toward the mediolateral junctions of neighboring cells; yellow arrows, cellular protrusions extended toward the neighboring cells; white and cyan lines, two different mediolateral junctions (equal length at the different timepoints); arrowheads, the ends of junctions. A, anterior; P, posterior; ML, mediolateral.

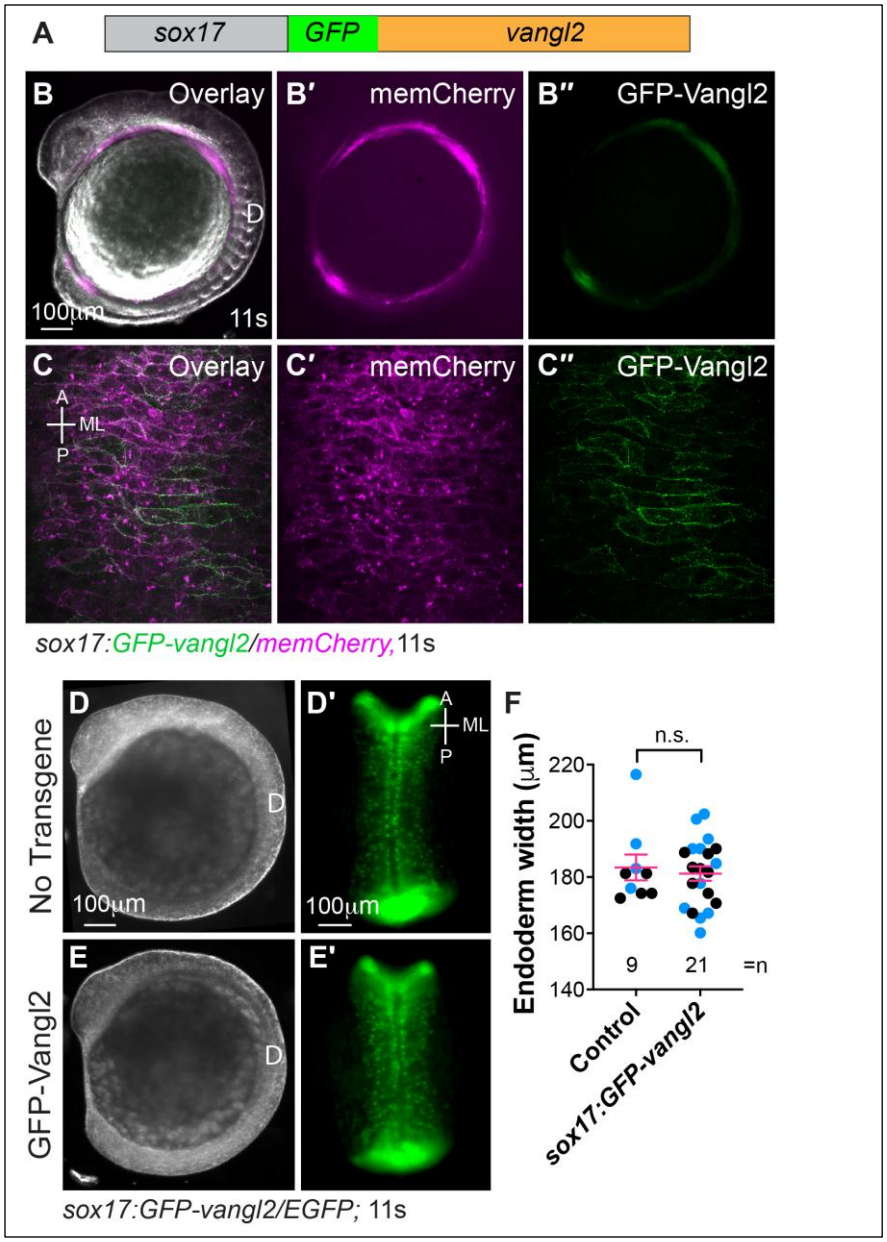

Fig. S6. Generation of the *Tg(sox17:GFP-vangl2)* line.

(A) Schematic of the zebrafish GFP-Vangl2 transgene under control by the endoderm-specific promoter *sox17* (gray box). (B-B′′) Lateral view of a live embryo expressing GFP-Vangl2 transgene; endoderm is labeled with memCherry. Overlay image of bright-field (B), epifluorescence of mCherry (B′) and GFP (B′′). (C-C′′) A confocal image (Z-projection) at 11s. Overlay (C) showing expression of mCherry (C′) and GFP-Vangl2 (C′′) on the plasma membranes of endodermal cells. (D-E′) Brightfield images (D, E, lateral view) and epifluorescence images of EGFP-labeled posterior endoderm (D′-E′, dorsal view) in the indicated embryos. (F) Average endoderm width in the indicated embryos from two independent experiments (represented by different color dots) with the number of embryos indicated. no significance or n.s., P >0.05; Unpaired two-tailed student's *t*-test. D, dorsal; A, anterior; P, posterior; ML, mediolateral.

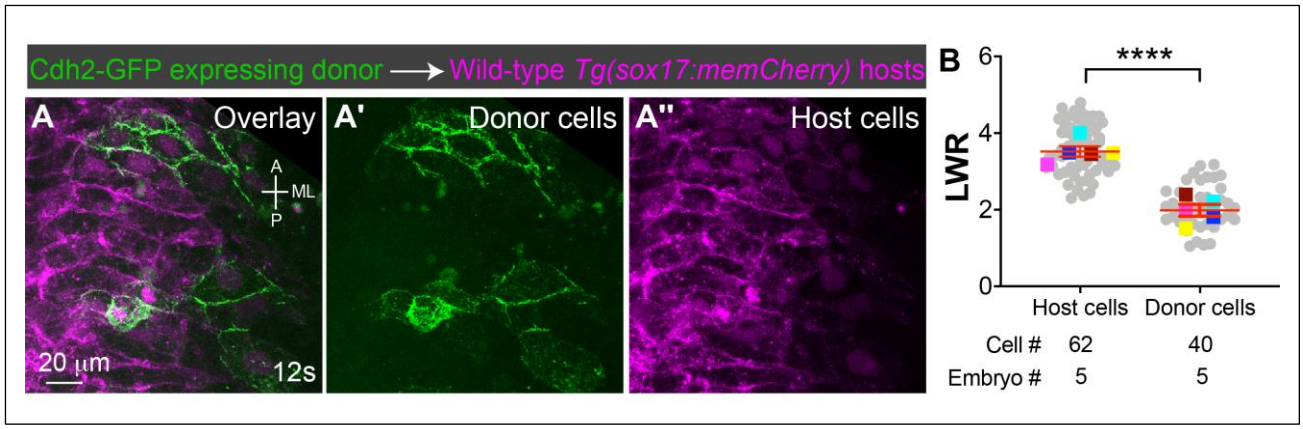

Fig. S7. Overexpression of Cdh2 in endodermal cells disrupts their cell polarity. (A-A'') Confocal images (Z-projections) showing Cdh2-overexpressing donor endodermal cells (green) in wild-type host endodermal cells. A, anterior; P, posterior; ML, mediolateral. (B) Average LWR of host and donor endodermal cells at 12s. Data from 5 chimeric embryos (represented by different color squares) and all cells (grey dots) are superimposed, with the number of cells and embryos indicated. ****, $P<0.0001$, Unpaired two-tailed student's *t*-test.

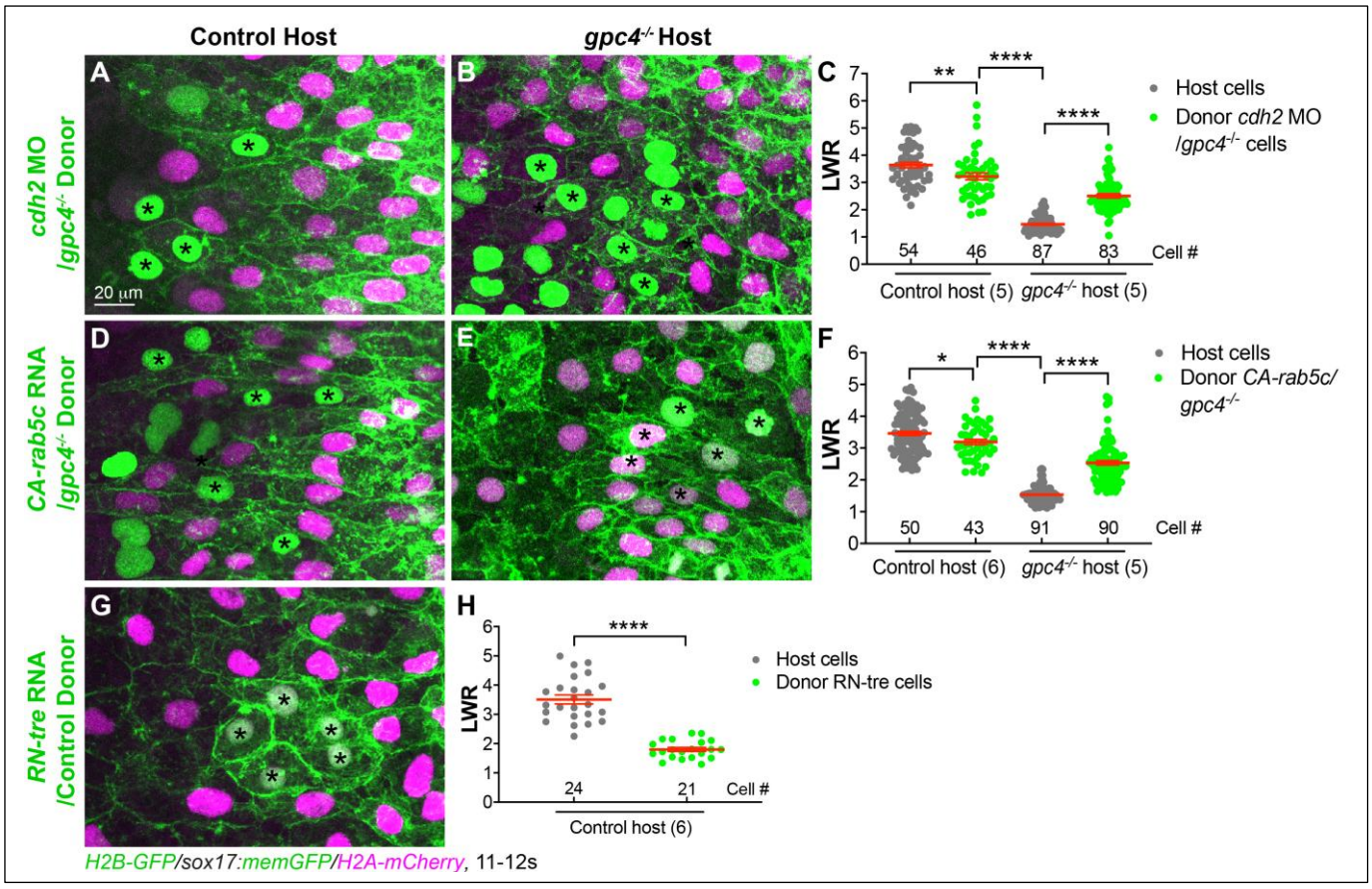

Fig. S8. Cell-autonomous functions of Gpc4, Rab5c and Cdh2 in regulating endodermal planar polarity. Transplantation was performed in the indicated embryos. (A,B,D,E,G) Confocal images (Z-projection) at XY view showing endodermal cells in the indicated host embryos transplanted with the indicated donor endoderm cells (whose nuclei are green, asterisk). (C,F,H) Graphs showing average LWR of host and donor endodermal cells in the indicated host embryos. All cells analyzed are plotted and the number of embryos and cells analyzed is shown. no significance or n.s., P >0.05; *, P <0.05; **, P <0.01; ****, P <0.0001; Unpaired two-tailed student's t-test.

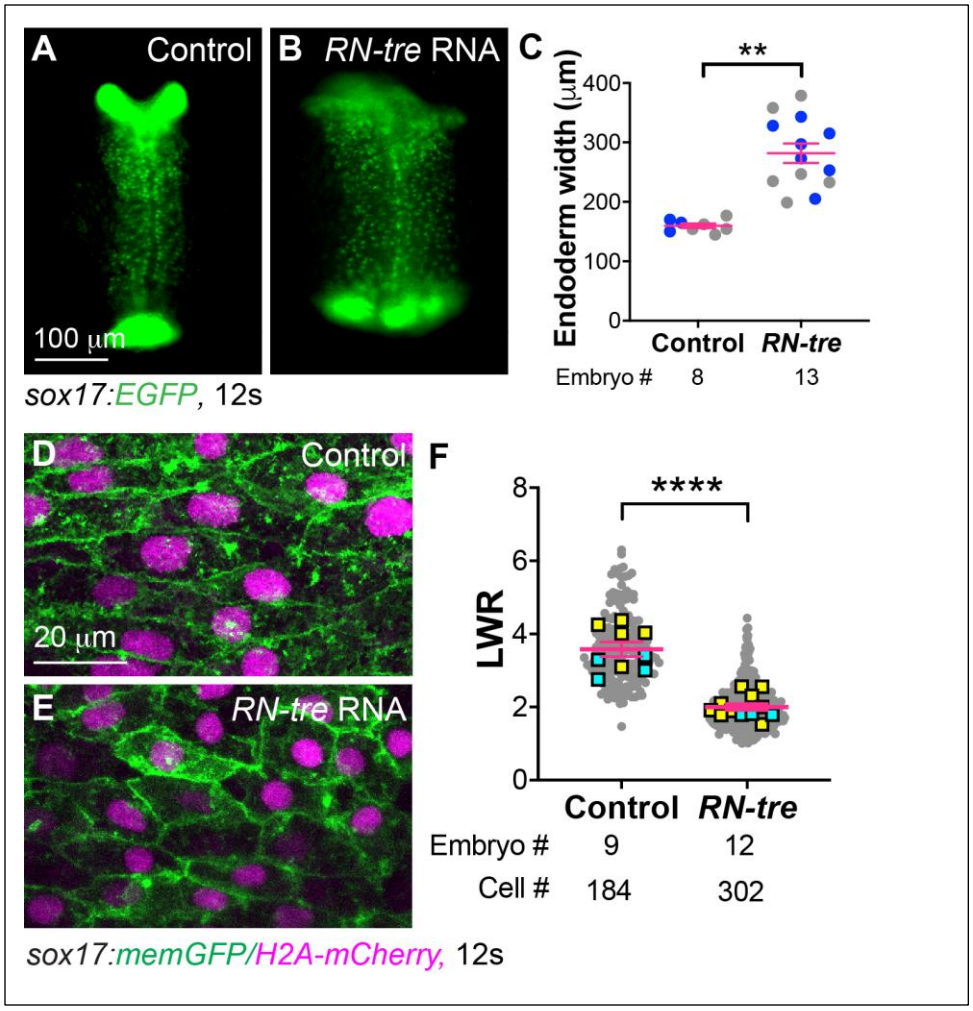

Fig. S9. Rab5 function is required for endodermal cell polarity and endoderm C&E. (A, B) Epifluorescence images of the posterior endoderm in uninjected or *RN-tre* mRNA injected embryos at the 12s. (C) Average posterior endoderm width in embryos shown in A, B. from two independent experiments (represented by different color dots) with the number of embryos and cells indicated. **, p<0.01, Student's *t*-test. (D, E) Confocal images (Z-projections) of XY view showing endodermal cells in the embryos. (F) Graph showing average LWR of endodermal cells in D, E. Data from all embryos (squares, different experiments are shown in different colors) and from all cells (grey circles) are superimposed, with number of cells and embryos indicated. ****, *P* <0.001, Unpaired two-tailed student's *t*-test.

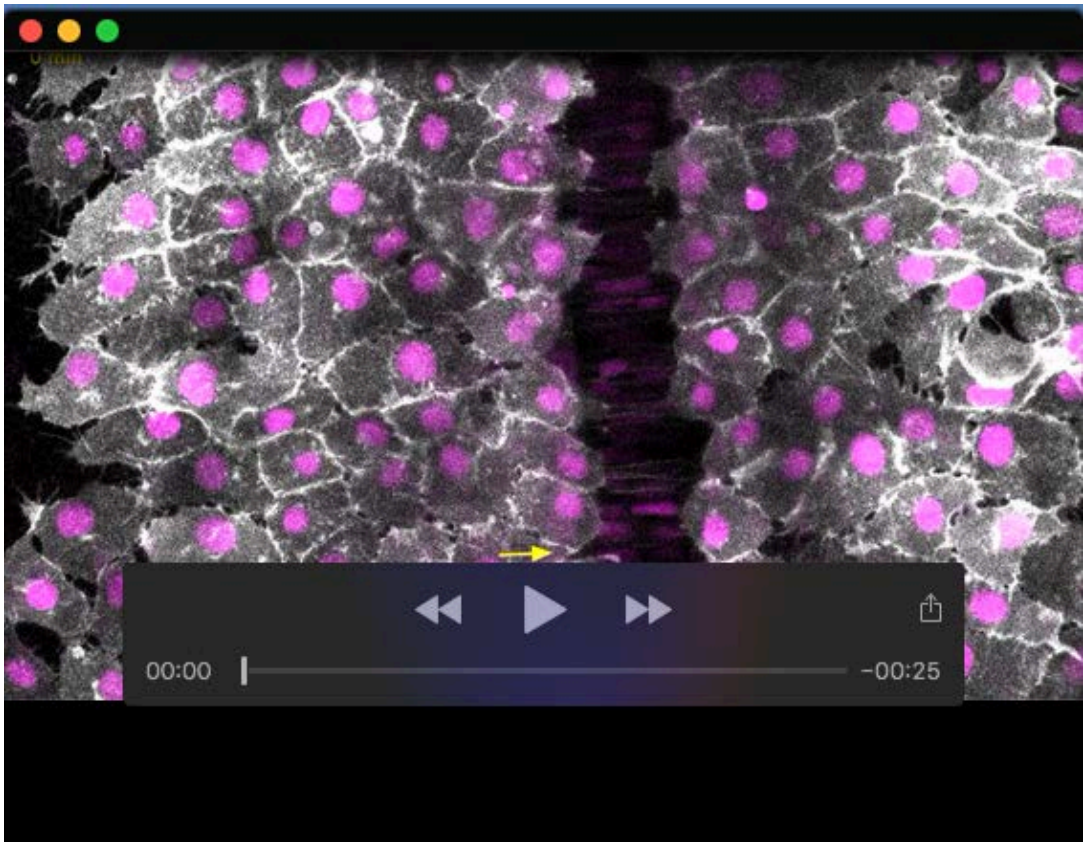

Movie 1. Endodermal cells display junctional changes and polarized cellular protrusions during endoderm C&E in control embryos at 7-12s.

Confocal time-lapse experiment was performed on *Tg(sox17:memGFP/H2A-mCherry)* embryos at 7-12s using Zeiss LSM880 confocal microscope with a LD C-Apo 20×/NA 0.8. Images were acquired at 5 min intervals and the movie plays at 4 frames/sec. Green lines: Type 3 junctions (T3), mediolaterally shrinking junctions; Red lines: Type 1 junctions (T1), anterior-posteriorly expanding junctions; Dashed yellow lines: rosettes; Yellow arrows: the leading edge of the endodermal cells that squeezed between neighboring cells; Green arrowheads: cellular protrusions in the leading edge of endoderm cells at the midline.

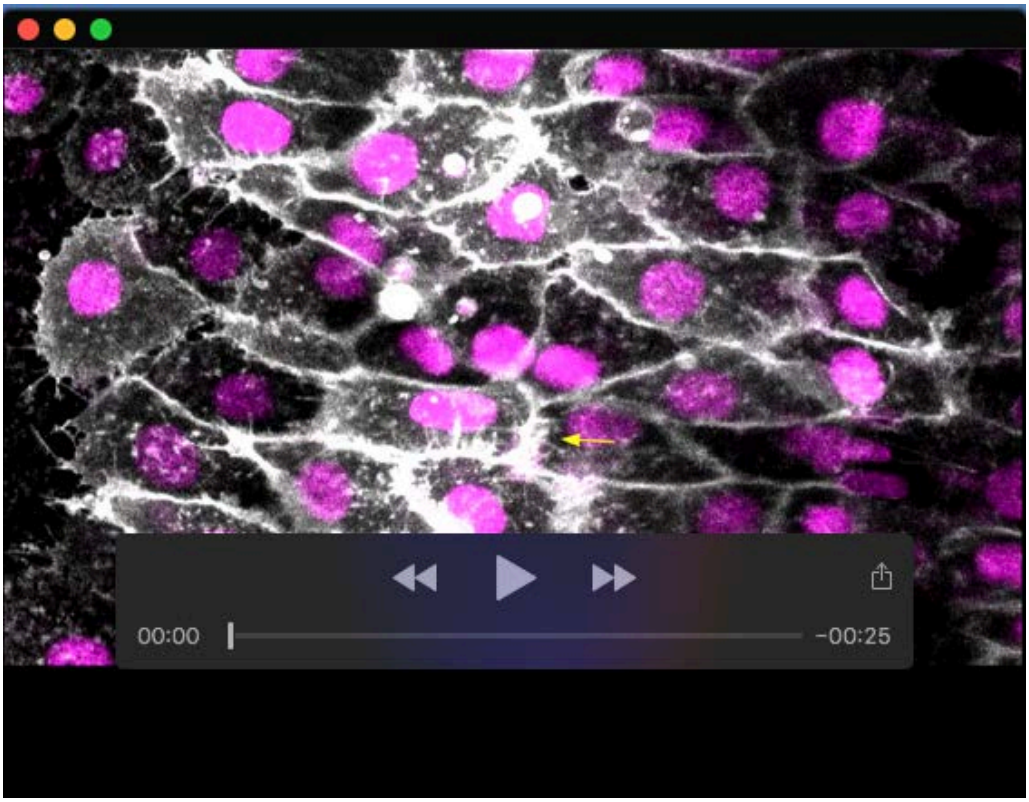

Movie 2. **Endodermal cells extended broad lamellipodia along ML axis in control embryos during 7-12s**.

Confocal time-lapse experiment was performed on *Tg(sox17:memGFP)* embryos at 7-12s using Zeiss LSM880 confocal microscope with a LD C-Apo 40×/NA 1.1 water objective at 1.4 zoom. Images were acquired at 15 sec intervals and the movie plays at 4 frames/sec. Yellow arrows: lamellipodial like protrusions.

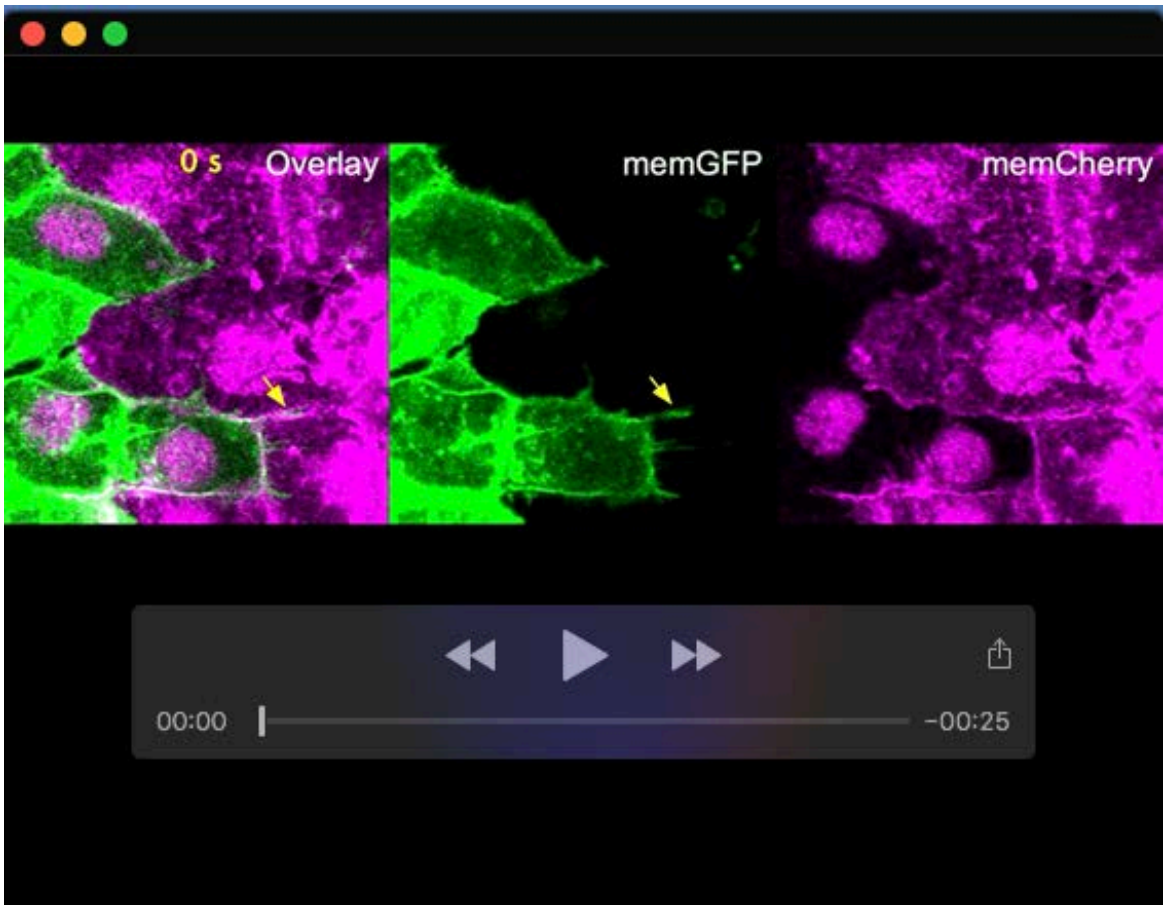

Movie 3. Junctional changes and polarized cellular protrusions occur in the same endodermal cells that are undergoing cell intercalations during 7-12s.
Donor cells from *Tg(sox17:H2A-Cherry)* embryos injected with *memGFP* and *sox32* RNAs were transplanted into *Tg(sox17: memCherry/H2A-Cherry)* host embryos. Time-lapse experiments were performed on the host embryos at 6s, in which the endoderm containing memGFP-expressing donor endoderm cells were imaged at 30s interval and movies play at 4 frames/sec. Yellow arrows: cells protrusions invading ML junctions that are shortening.

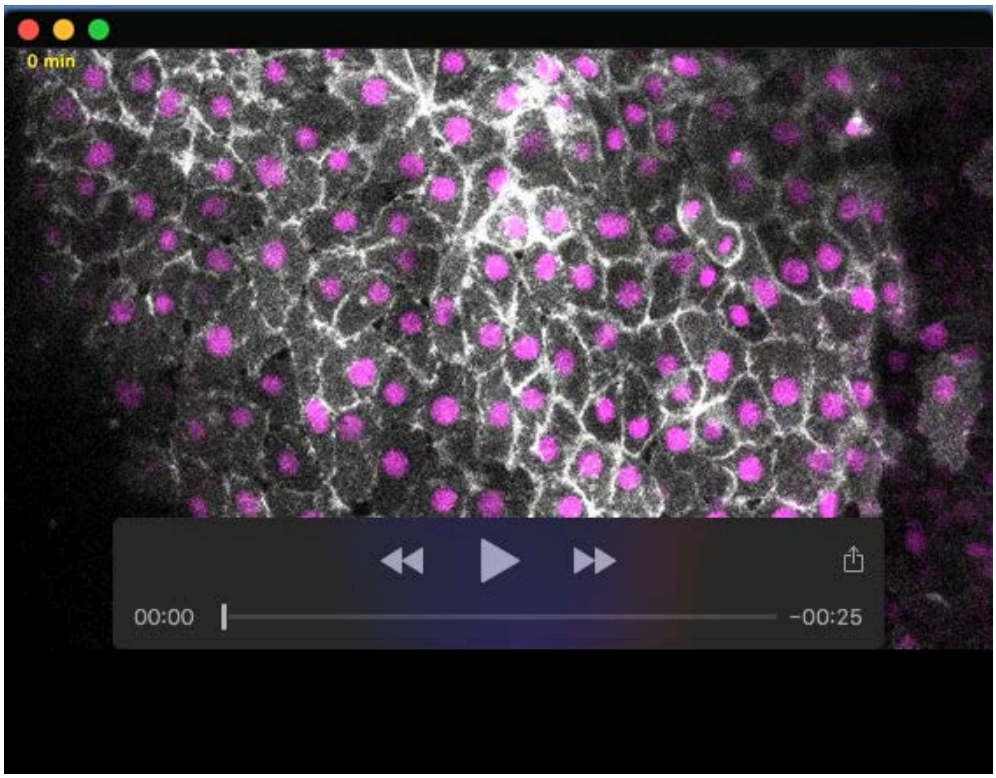

Movie 4. **Endodermal cells display junctional changes but not polarized cellular protrusions during endoderm C&E in *gpc4*$^{-/-}$ mutant embryos during 7-12s.** Confocal time-lapse experiment was performed on *gpc4*$^{-/-}$*/Tg(sox17:memGFP/H2A-mCherry)* embryos using the same settings with that in Movie 1 and the movie plays at 4 frames/sec. Labeling in this movie is the same as that of Movie 1.

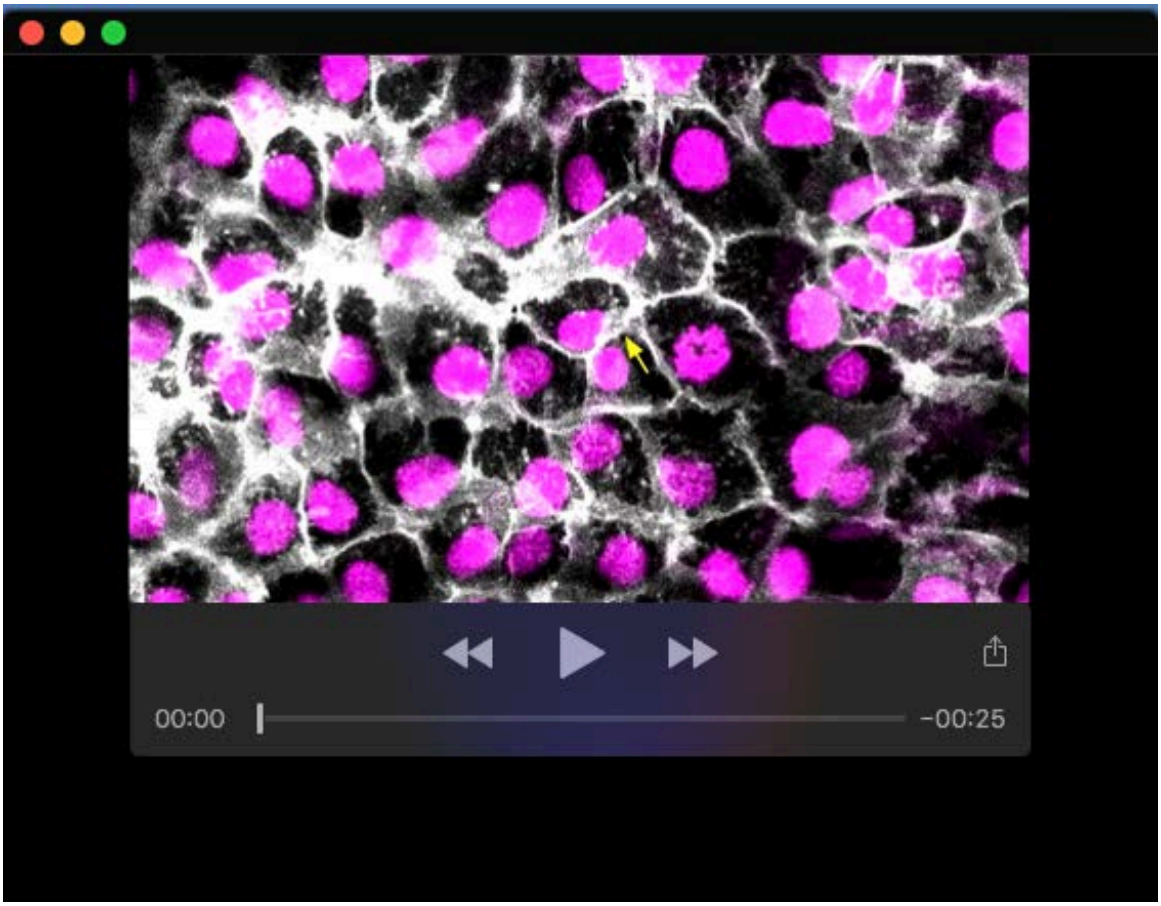

Movie 5. **Endodermal cells extended lamellipodia in random directions in *gpc4*$^{-/-}$ embryos at 7-12s.**

Confocal time-lapse experiment was performed on *gpc4*$^{-/-}$*/Tg(sox17:memGFP)* embryos using the same settings with that in Movie 2 and the movie plays at 4 frames/sec. Labeling in this movie is the same as that of Movie 2.